

Vision Transformers for Zero-Shot Clustering of Animal Images: A Comparative Benchmarking Study

Hugo Markoff¹ | Stefan Hein Bengtson² | Michael Ørsted¹

¹Department of Chemistry and Bioscience, Aalborg University, Aalborg, Denmark

²Department of Architecture, Design and Media Technology, Visual Analysis and Perception Lab, Aalborg University, Aalborg, Denmark

Correspondence

Corresponding author Hugo Markoff, Department of Chemistry and Bioscience, Aalborg University, Aalborg, Denmark.

Email: khbm@bio.aau.dk

Abstract

Manual labeling of animal images remains a significant bottleneck in ecological research, limiting the scale and efficiency of biodiversity monitoring efforts. This study investigates whether state-of-the-art Vision Transformer (ViT) foundation models can reduce thousands of unlabeled animal images directly to species-level clusters. We present a comprehensive benchmarking framework evaluating five ViT models combined with five dimensionality reduction techniques and four clustering algorithms, two supervised and two unsupervised, across 60 species (30 mammals and 30 birds), with each test using a random subset of 200 validated images per species. We investigate when clustering succeeds at species-level, where it fails, and whether clustering within the species-level reveals ecologically meaningful patterns such as sex, age, or phenotypic variation. Our results demonstrate near-perfect species-level clustering (V-measure: 0.958) using DINOv3 embeddings with t-SNE and supervised hierarchical clustering methods. Unsupervised approaches achieve competitive performance (0.943) while requiring no prior species knowledge, rejecting only 1.14% of images as outliers requiring expert review. We further demonstrate robustness to realistic long-tailed distributions of species and show that intentional over-clustering can reliably extract intra-specific variation including age classes, sexual dimorphism, and pelage differences. We introduce an open-source benchmarking toolkit and provide recommendations for ecologists to select appropriate methods for sorting their specific taxonomic groups and data.

KEY WORDS

Vision Transformers, camera trap images, zero-shot clustering, biodiversity monitoring, species identification, foundation models, ecological applications

Preprint Notice: This manuscript is a preprint and has not undergone peer review. The authors retain copyright in this work.

1 | INTRODUCTION

Biodiversity monitoring has entered a critical phase where the volume of visual data generated through camera traps, citizen science platforms, and research expeditions exceeds our capacity for manual analysis Weinstein (2018). At the same time, global wildlife populations are plummeting, where recent estimates suggest that monitored vertebrate populations have declined by 73% in the past five decades, making efficient and accurate species monitoring more crucial than

ever WWF (2024). Traditional approaches to animal image classification rely heavily on expert knowledge and manual annotation, creating a significant bottleneck in ecological research workflows.

With individual studies generating hundreds of thousands to millions of images annually, the volume of data fundamentally limits the scale and timeliness of biodiversity assessments if labeling of the data has to be done manually Norouzzadeh et al. (2021). Figure 1 illustrates the core objective of this work: transforming an unordered collection of animal images into coherent species-level clusters without manual annotation.

Current solutions often employ supervised learning approaches, such as Convolutional Neural Networks (CNNs), which are trained on large labeled datasets to classify species Beery et al. (2019), Gadot et al. (2024a). Binary animal classification models for automatic camera systems, in different domains, terrestrial mammals, birds, fishes and insects manage

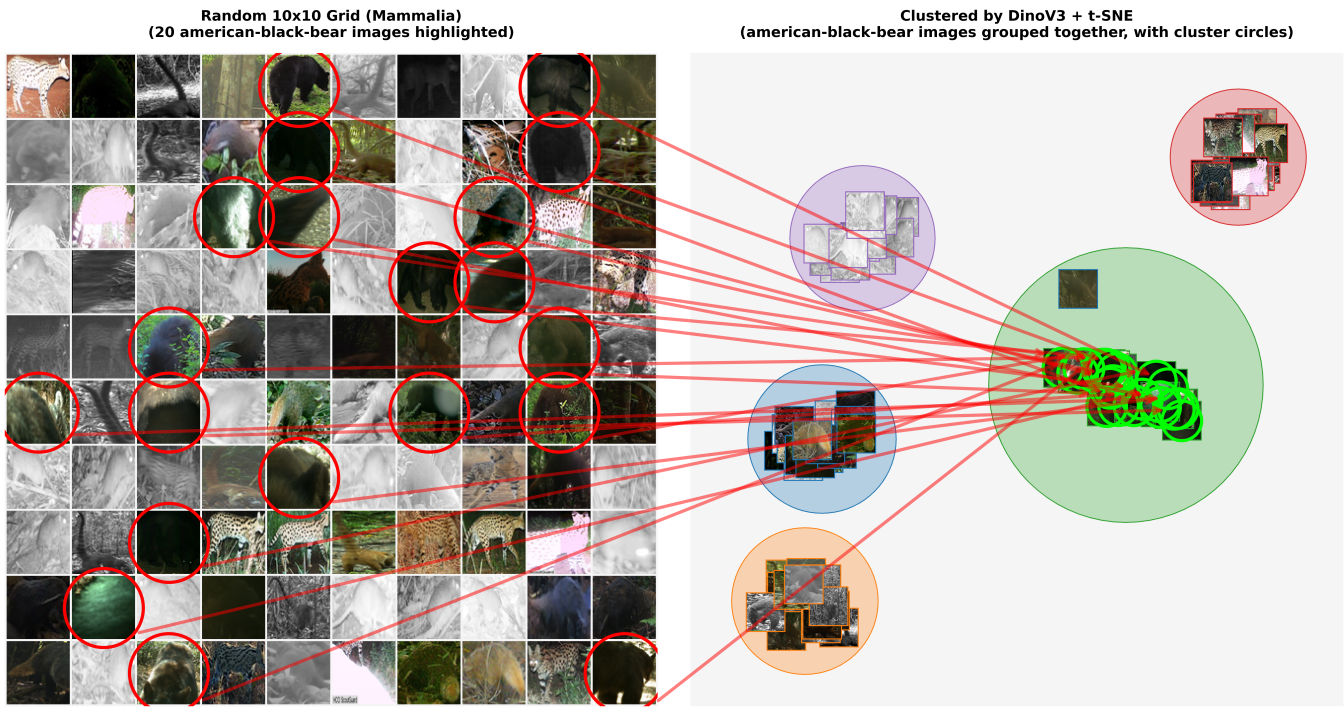


FIGURE 1 Left side; 100 randomly ordered images from 5 mammal classes. Right side; images sorted in 2-D embedding space clusters, from results of DINOV3, t-SNE and HDBSCAN.

to achieve high accuracy in detecting solely the presence of animals in images.

These detection models include MegaDetector Beery et al. (2019) for terrestrial mammals and birds, Community Fish Detector (CFD) WildHackers (2025) for fishes, and FlatBug Svenning et al. (2025) for insects. These models show great potential for grounding the input for species-level classification models, by cropping out the area of interest, where an animal is present. There have already been classifiers developed with this pipeline, where MegaDetector is used to crop parts of the image where an animal is present, and passing the croppings to a species-level classification model, such as DeepFaune Rigoudy et al. (2023) and SpeciesNet Gadot et al. (2024a).

While achieving high accuracy on well-represented species and domains, supervised deep learning perpetuates an annotation bottleneck: thousands of images must be manually labeled before models become useful Norouzzadeh et al. (2021). Furthermore, supervised classifiers are inherently limited to a fixed set of species present in the training data Vyskočil and Picek (2024) and struggle with the typical long-tailed distribution of biodiversity, where a few common species dominate, while many rare or threatened taxa have insufficient training examples Pantazis et al. (2021). This is especially problematic as the rarer species are often important and the lack of the sufficient training data may cause them to be wrongly classified. Furthermore, supervised classifiers trained on limited datasets can overfit to

specific domains, failing to generalize to new sites with different backgrounds, imaging conditions, or species Beery et al. (2018b), Norouzzadeh et al. (2021), limiting their real-world applicability. These constraints create a need for methods that can organize and interpret unlabeled animal imagery without extensive species-specific training.

Recent advances in Vision Transformer (ViT) foundation models, particularly those trained on large-scale biological datasets such as BioCLIP Stevens et al. (2024) and BioCLIP 2 Gu et al. (2025), have demonstrated zero-shot classification capabilities by learning visual representations from millions of species images. However, there exists a critical gap between demonstrated classification performance and practical deployment scenarios, such as usage in autonomous camera systems. For instance, BioCLIP 2 states a 54% species-level accuracy for the IDLE-OO-Camera-Traps dataset Gu et al. (2025), meaning that for the remaining 46% of images, extensive manual validation is still required.

Lowe and Haurum (2024) demonstrated the feasibility of zero-shot clustering for ecological images, showing that image embeddings from pretrained models, such as self-supervised ViT ones, can form well-defined clusters, even on unseen fine-grained biodiversity datasets such as species from iNaturalist.

1.1 | Our contribution

In this paper, we approach the problem from a practical ecological perspective, moving beyond feasibility demonstrations to address real-world deployment needs. Rather than testing whether models can match individual images to pre-defined species labels, we examine whether learned representations naturally separate images by species when no prior labels are available. We systematically benchmark combinations of foundation models, dimensionality reduction techniques, and clustering algorithms to provide results from different combinations of model and method selections. We also investigate when these methods fail and whether clustering failures reveal biologically meaningful patterns (sex dimorphism, age classes, seasonal fur changes) versus model limitations. This work aims to provide results to better understand when clustering can reduce annotation burden, when it reveals intra-species variation, and when manual validation remains essential.

Our work addresses these gaps through four primary contributions:

- 1. Comprehensive benchmarking framework:** We systematically evaluate 5 state-of-the-art ViT models \times 5 dimensionality reduction approaches \times 4 clustering algorithms across a total of 60 species from two taxonomic classes (Mammals and Birds), providing quantitative performance metrics for thousands of method combinations and results to select best-performing combinations.
- 2. Validated animal dataset:** We provide an open-source dataset consisting of 139,111 manually validated image crops across all 60 species, each processed through automated detection pipelines that mirror real-world workflows and enables benchmarking for future research.
- 3. Ecological interpretation framework:** Beyond quantitative metrics, we analyze clustering compositions to distinguish when “failures” represent genuine ecological subcategories (intra-species variation or environmental context with biological meaning) versus pure model limitations, providing insights for practical deployment and expert validation strategies.
- 4. Open-source toolkit and visualization website:** We release complete code, dataset, logged results from all experimental runs, and an interactive web interface, enabling ecologists to explore method combinations and visualize clustering results without coding expertise.
- 5. Practical deployment guidelines:** Based on our empirical results, we provide concrete recommendations for parameter selection tailored to dataset characteristics, including guidance for large versus small datasets, handling long-tailed species distributions, and prioritizing rare species detection for expert review.

Our approach explicitly targets the practical needs of ecological researchers: reducing annotation burden, handling taxonomic uncertainty, prioritizing expert attention on ambiguous edge-cases, and understanding when automated methods can be trusted versus when manual validation remains essential.

2 | RELATED WORK

2.1 | Vision transformers in computer vision

Vision Transformers, introduced by Dosovitskiy et al. (2021) revolutionized computer vision by adapting the transformer architecture from natural language processing to image analysis. By treating images as sequences of patches and applying self-attention mechanisms, ViTs achieved competitive performance with CNNs while offering better interpretability and scalability. The success of ViTs has led to numerous variants optimized for specific applications and computational constraints.

CLIP (Contrastive Language-Image Pre-training) Radford et al. (2021) demonstrated the power of multimodal learning by jointly training vision and language models on large-scale internet data. This approach enabled zero-shot classification capabilities, where models could classify images based on natural language descriptions without task-specific training. SigLIP Zhai et al. (2023) improved upon CLIP’s training efficiency through sigmoid-based contrastive learning, achieving better performance with reduced computational requirements.

Self-supervised learning approaches like DINOv2 Oquab et al. (2023) have shown capabilities in learning visual representations without manually-defined labels. Instead, these models rely on automatically generating pseudo-labels and learn from these in a supervised manner. These models excel at capturing semantic relationships between images, making them particularly suitable for clustering and similarity-based tasks.

2.2 | Biological foundation models

Stevens et al. (2024) marked a significant advance by training on TreeOfLife-10M, a dataset containing images of over 454,000 taxa. The model achieved 16-17% improvements over general-purpose CLIP in taxonomic classification tasks. Critically, BioCLIP demonstrated zero-shot capabilities: identifying species it had never seen during training by leveraging taxonomic relationships learned from related species.

Gu et al. (2025) scaled to TreeOfLife-200M and introduced hierarchical contrastive learning that models taxonomic structure. Beyond classification improvements (18.1% over BioCLIP), the model exhibited emergent properties as training scaled. They found that the internal feature embeddings of the model aligned with ecological and functional relationships; for

example, freshwater and non-freshwater fish naturally separated in the embedding space of the model. Intra-species variations such as different life stages were also preserved within some subspaces.

Recent work by Gadot et al. (2024b) demonstrated that cropping to bounding boxes improves classification performance compared to whole-image analysis. This pre-processing step reduces background noise and focuses attention on animal features. Detection models like MegaDetector have achieved near-perfect accuracy for binary animal detection in camera trap images, making automated cropping pipelines practical for large-scale studies.

2.3 | Clustering and dimension reduction

Recent work by Lowe and Haurum (2024) addressed zero-shot clustering using ViT embeddings for different datasets, including biological image data, demonstrating the feasibility of using zero-shot clustering methods.

Dimensionality reduction techniques such as UMAP McInnes et al. (2018), t-SNE van der Maaten and Hinton (2008), and PCA offer different trade-offs between preserving local structure, global relationships, and computational efficiency. UMAP has been adopted in single-cell transcriptomics Becht et al. (2019) and other biological applications due to its computational efficiency and ability to preserve both local and global structure McInnes et al. (2018). In contrast, t-SNE excels at revealing local clustering patterns van der Maaten and Hinton (2008) but can distort distances between distant clusters and is computationally more intensive than UMAP Kobak and Berens (2019).

Clustering algorithm selection poses additional challenges. Density-based methods such as DBSCAN and HDBSCAN Campello et al. (2013) can determine cluster numbers based on data density without requiring pre-specification of the number of estimated clusters. Hierarchical clustering provides interpretable dendograms but exhibits computational complexity depending on linkage method and implementation Abboud et al. (2019), limiting scalability to large datasets. Gaussian Mixture Models (GMM) Reynolds (2009) handle overlapping clusters probabilistically by assuming specific distributional forms. While clustering algorithms have been evaluated on various types of embeddings, systematic evaluations establishing optimal combinations for deep learning embeddings in camera trap species identification remain limited.

3 | METHODOLOGY

Our methodology consists of two distinct pipelines: (1) dataset preparation, where we collect and manually validate camera

trap images to establish ground truth labels, and (2) zero-shot clustering, where we systematically evaluate and benchmark combinations of ViT models, dimensionality reduction techniques, and clustering algorithms. This section describes both pipelines and our evaluation framework.

3.1 | Dataset Preparation Pipeline

Our dataset preparation pipeline, illustrated in Figure 2, established the ground truth labels for evaluating the zero-shot clustering methods. An initial total of 281,127 raw camera trap images from 60 different species were selected. We applied automated detection and cropping, followed by expert validation, resulting in 139,111 manually validated species-level crops spanning from 461 to 6,831 images per species (Table B1, Appendix B).

3.1.1 | Species selection and image extraction

We selected the 60 species (30 mammal and 30 bird species) based on three criteria: (1) sufficient raw data ($\geq 3,000$ candidate images across multiple projects), (2) representation of diverse geographic regions and ecosystems, and (3) varied morphological characteristics across species. All images were sourced from 23 camera trap projects within LILA BC (Labeled Information Library of Alexandria: Biology and Conservation) LILA (2018), a repository containing over 10 million images from worldwide camera trap deployments. Projects selected for our dataset can be seen in Table 1.

TABLE 1 Dataset Source Abbreviations

Code	Dataset
CAL	Caltech Camera Traps Beery et al. (2018a)
DLC	Desert Lion Camera Traps des (2024)
ENA	ENA24 Detection Yousif et al. (2019)
ICT	Idaho Camera Traps Idaho Dep. of Fish and Game (2024)
ISC	Island Conservation isl (2024)
MIS	Missouri Camera Traps Zhang et al. (2016)
NAC	NACTI Tabak et al. (2019)
NKC	Nkhotakota Camera Traps Appel et al. (2025)
NZC	New Zealand Camera Traps new (2024)
OSU	OSU Small Animals Balasubramaniam (2024)
SCD	Snapshot Camdeboo sna (2024a)
SEN	Snapshot Enonkishu sna (2024b)
SIC	Seattle-ish Camera Traps Morris (2024)
SKA	Snapshot Karoo sna (2024c)
SKG	Snapshot Kgalagadi sna (2024d)
SKR	Snapshot Kruger sna (2024e)
SMZ	Snapshot Mountain Zebra sna (2024f)
SS24	Snapshot Safari 2024 sna (2024g)
SSE	Snapshot Serengeti Swanson et al. (2015)
SWG	SWG Camera Traps SWG (2021)
UNS	UNSW Predators uns (2024)
WCS	WCS Camera Traps Wildlife Conservation Society (2024)
WLC	Wellington Camera Traps Anton et al. (2018)

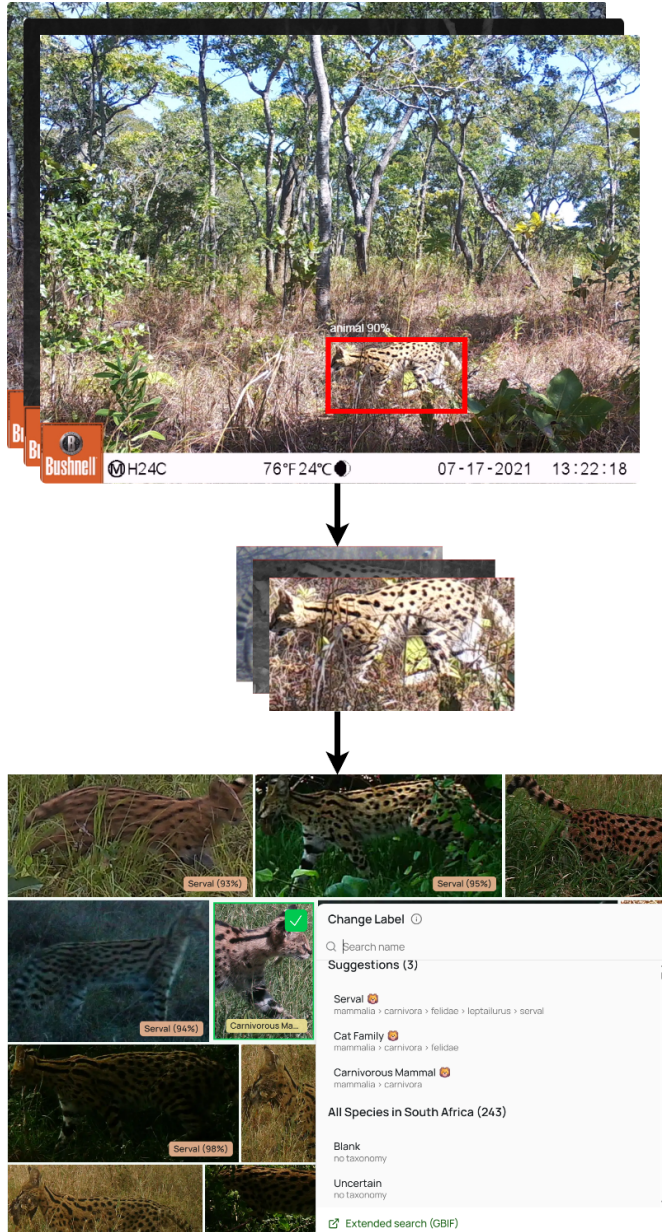


FIGURE 2 Data preparation pipeline using the Animal Detect platform. First step using the MegaDetector1000 Redwood model to detect animals, shown with red bounding boxes. Second step, cropping the images, using the bounding box location and third step with expert validation, ensuring the classifications are correct, re-labeling uncertain cases.

To handle taxonomic inconsistencies across projects, we developed a unification tool that standardized species labels within the 23 projects. For species with more than 5,000 available images, the tool randomly sampled images, while species with fewer images included all available samples. With this multi-project sampling we attempt to create a heterogeneous dataset with images from different camera models, environmental backgrounds, lighting conditions, and animal poses. From the 60 selected species, we initially selected 281,127 raw images for processing. The complete species list, and the number of validated images, with sources is provided in Appendix B.

3.1.2 | Detection and cropping

Raw images were processed through the Animal Detect platform Markoff and Galaktionovs (2025a), where a simplified pipeline is illustrated in Figure 2, which implements:

Detection stage: The MegaDetector1000 Redwood model, Beery et al. (2019), identifies bounding boxes for animals in images. MegaDetector achieves high recall for mammal and bird detection in camera trap imagery, enabling reliable automated processing.

Classification stage: Detected regions are classified using SpeciesNet combined with Animal Detect's hierarchical re-classification logic Markoff and Galaktionovs (2025b), producing taxonomic predictions from kingdom to species-level with associated confidence scores.

Cropping: Images are cropped to bounding box coordinates following best practices established by Gadot et al. (2024b), where the cropped images are used in the zero-shot clustering pipeline, instead of the whole image.

Many images initially labeled with species annotations in LILA BC were filtered as empty during this stage. This occurred primarily due to camera burst mode, where a sequence of rapid-fire images receives the same species label even though the animal may only appear in one or two frames. Additionally, some images contained mislabeling in the original datasets. The pipeline intentionally retains challenging cases including partial occlusions, low-light conditions, motion blur, and images capturing only parts of animals (tails, legs, faces), reflecting real-world camera trap data quality.

Since the detection and cropping pipeline processes each bounding box independently, raw images containing multiple individuals of the same species would produce multiple crops.

3.1.3 | Expert validation

An ecologist with expertise in mammal and bird identification validated all the resulting image crops, verifying species-level identifications, while re-labeling very ambiguous cases as "uncertain".

This validation process resulted in a final dataset of 139,111 species-level crops, ranging from 461 to 6,831 images per species. Of these, 138,024 images (99.2%) were confirmed at species-level, while 1,087 images (0.8%) were marked as uncertain due to occlusion, blur, or ambiguous features. Both validated and uncertain images are included in the released dataset. The complete per-species breakdown of validated and uncertain images is provided in Table B1 (Appendix B).

3.2 | Zero-Shot clustering pipeline

The zero-shot clustering pipeline provides a modular framework for organizing unlabeled animal images into clusters. The primary aim of the zero-shot pipeline is to cluster cropped animal images that have been through data preprocessing as explained in Section 3.1 into homogeneous clusters, representing species-level groups, without requiring labeled training data. The pipeline, seen in Figure 3 starts with cropped image detections, followed with three sequential stages that can be configured with different methods depending on available resources and analytical goals.

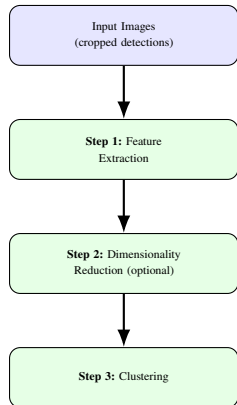


FIGURE 3 Zero-shot clustering pipeline architecture. Each stage is modular, allowing substitution of different models and methods as new approaches emerge.

Step 1: Feature extraction. Input cropped images of animals are passed through a pre-trained vision model to generate high-dimensional embedding vectors that capture visual semantics. The pipeline accepts models capable of producing fixed-length embeddings from images such as ViT models, hereunder different versions of DINO and CLIP, where the general purpose models would need no fine-tuning or task-specific training, enabling true zero-shot application.

Step 2: Dimensionality reduction (optional). High-dimensional embeddings can be projected to lower-dimensional spaces before clustering. This step serves two purposes: (1)

potential improvement of clustering algorithm performance by focusing on relevant structure while reducing noise and computational complexity, and (2) enabling 2D/3D visualization for manual inspection. The target dimensionality can be configured based on downstream requirements, from 2D for visualization to higher dimensions that preserve more information. Clustering directly on original embeddings is also supported.

Step 3: Clustering. The embedding space is partitioned using clustering algorithms. *Unsupervised methods* automatically determine cluster count based on data geometry, suitable when species richness is unknown. *Supervised methods* require pre-specification of cluster count, suitable when approximate species count is known.

3.2.1 | Clustering granularity and extensibility

The pipeline’s output granularity depends on configuration choices and the underlying embedding quality. With appropriate settings, clusters could be used to approximate species-level groupings. However, the framework also supports finer-grained clustering that may reveal intra-specific variation such as sexual dimorphism, age classes, or phenotypic variants. This flexibility allows ecologists to tune the pipeline toward their specific analytical goals, from coarse taxonomic sorting to detailed population structure analysis. Higher cluster counts typically yield higher homogeneity (purer clusters) at the cost of splitting single species across multiple groups.

The modular design ensures the pipeline remains relevant as new methods emerge. Any component can be substituted without modifying other stages: new foundation models can replace the feature extractor, novel dimensionality reduction techniques can be incorporated, and alternative clustering algorithms can be evaluated. We release both the pipeline implementation and benchmarking code to facilitate extension with future methods (Section 6).

3.3 | Benchmarking Framework

To evaluate the zero-shot clustering pipeline, we designed a benchmarking framework that systematically tests combinations of embedding models, dimensionality reduction methods, and clustering algorithms across multiple experimental runs.

3.3.1 | Experimental Design

The benchmarking framework seen in Figure 4 follows a factorial design, evaluating every combination of pipeline components to identify optimal configurations and understand component interactions.

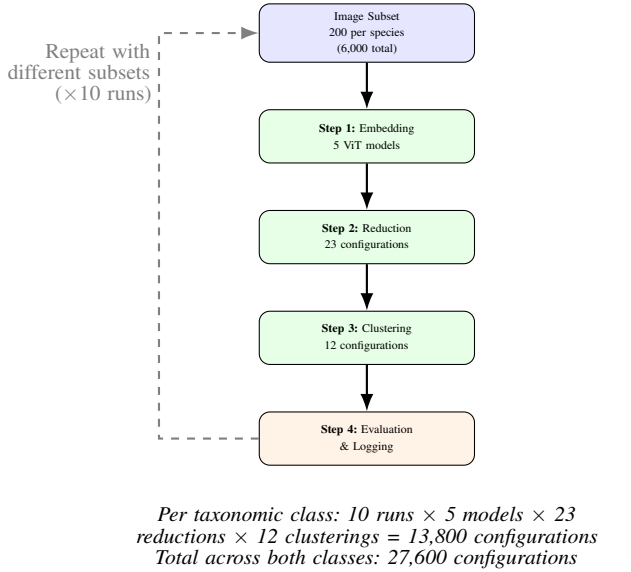


FIGURE 4 Benchmarking framework architecture. The complete pipeline is repeated 10 times for mammals and 10 for birds, with different random image subsets to generalize beyond a single specific sample selection.

Image Sampling. For each experimental run, we randomly sample 200 validated images per species within each taxonomic class (mammals or birds), yielding 6,000 images per run (30 species \times 200 images).

Experimental Scale. This benchmarking design evaluates:

$$10 \text{ runs} \times \underbrace{5 \text{ ViT models}}_{\text{dim. red. configs}} \times \underbrace{23}_{\text{clustering configs}} = 13,800 \text{ configurations}$$

Additionally, clustering directly on original high-dimensional embeddings adds $10 \times 5 \times 12 = 600$ per class. The complete benchmark totals **28,800 configurations** across both taxonomic classes.

3.3.2 | Vision Transformer Models

We evaluate five state-of-the-art Vision Transformer models (Table 2) representing different training paradigms: general-purpose vision-language models (CLIP, SigLIP), self-supervised models (DINOv2, DINOv3), and a biology-specific

model (BioCLIP 2). All models use publicly available pre-trained weights without fine-tuning, ensuring true zero-shot evaluation.

TABLE 2 Vision Transformer Models Evaluated

Model	Parameters	Embedding Dim
CLIP (ViT-L/14) ^a	304M	768
SigLIP (ViT-B/16) ^b	200M	768
DINOv2 (ViT-g/14) ^c	1,100M	1536
DINOv3 (ViT-H+/16) ^d	840M	1280
BioCLIP 2 (ViT-L/14) ^e	304M	768

^aRadford et al. (2021), ^bZhai et al. (2023), ^cOquab et al. (2023),

^dSiméoni et al. (2025), ^eGu et al. (2025)

All sampled images are processed through each model to generate high-dimensional embedding vectors (768D–1536D depending on architecture). The embedding vector is extracted as the image representation, capturing global visual semantics.

3.3.3 | Dimensionality reduction techniques

High-dimensional embeddings (768D–1536D) are projected to 2D spaces. While dimensionality reduction may improve clustering performance by reducing noise and computational complexity, the primary motivation for 2D projection is enabling visualization for manual inspection for downstream evaluation tasks. We evaluate two non-linear methods alongside three deterministic. Each embedding set undergoes 23 reduction configurations:

Non-deterministic methods (10 runs each):

- **UMAP** (Uniform Manifold Approximation and Projection): Preserves both local and global structure through Riemannian geometry. Parameters: `n_neighbors=15, min_dist=0.1, metric='euclidean', n_components=2`. Run 10 times with different random seeds to capture stochastic variation.
- **t-SNE** (t-distributed Stochastic Neighbor Embedding): Emphasizes local neighborhood structure through probability distributions. Parameters: `perplexity=30, learning_rate='auto', init='pca', n_components=2`. Run 10 times with different random seeds to capture stochastic variation.

Deterministic methods (1 run each):

- **PCA** (Principal Component Analysis): Linear projection capturing maximum variance. Provides interpretable baseline for non-linear methods.
- **Isomap** (Isometric Feature Mapping): Non-linear projection preserving geodesic distances along the data manifold.

- **Kernel PCA:** Non-linear projection using Radial Basis Function (RBF) kernel to capture complex relationships in feature space.

All embeddings are standardized using `StandardScaler` before reduction. Additionally, we evaluate clustering directly on original high-dimensional embeddings, with no reduction, bringing the total to 24 embedding space configurations per model.

3.3.4 | Clustering algorithms

Each reduced embedding space is partitioned using four clustering algorithms representing two paradigms: unsupervised methods that autonomously discover cluster structure, and supervised methods requiring pre-specification of cluster count. This dual approach benchmarks both realistic field scenarios (unknown species counts) and informed scenarios (known approximate species richness).

Unsupervised Methods (2 configurations):

These algorithms automatically determine cluster count and structure based on embedding geometry, suitable for exploratory analyses where species count is unknown. Parameters were set using principled defaults rather than dataset-specific tuning to minimize bias and enable transfer to other ecological applications:

- **DBSCAN** (Density-Based Spatial Clustering): Groups points based on local density without requiring cluster count specification. Parameters: `min_samples=5, eps` estimated automatically per dataset using the k-nearest neighbors heuristic. This automatic estimation adapts to the natural scale of each embedding space while reducing manual tuning requirements.
- **HDBSCAN** (Hierarchical DBSCAN): Builds a hierarchy of density-based clusters and extracts stable clusters at varying densities. Parameters: `min_cluster_size=15, min_samples=5`. The minimum cluster size of 15 reflects the practical consideration that smaller clusters are difficult to validate ecologically and may represent outliers rather than genuine species groupings.

Both density-based methods produce **outlier labels** (–1) for points not meeting density criteria. In zero-shot clustering workflows, these outlier-labeled images require manual expert review, representing a trade-off between automated clustering and validation burden.

Supervised Methods (10 configurations):

These algorithms require pre-specification of cluster count, enabling systematic investigation of how incorrect species richness estimation affects performance. We evaluate multiple

values: $k \in \{15, 30, 45, 90, 180\}$, where $k = 30$ represents the true species count. This range serves dual purposes:

1. *Performance degradation quantification:* Assess how clustering quality degrades when species richness estimates deviate from ground truth, spanning from half to six times the true count to capture estimation errors.
2. *Ecological interpretation:* Enable post-hoc analysis of cluster compositions. Under-splitting ($k < 30$) may reveal whether embeddings group species by higher taxonomic levels (e.g., families like cat family or deer family), while over-splitting ($k > 30$) may expose biologically meaningful intra-specific variation such as sexual dimorphism, age classes, seasonal pelage/plumage differences, or individual pattern variation.

Two complementary algorithms are evaluated at each k value:

- **Hierarchical Clustering:** Agglomerative clustering with Ward linkage. Produces dendograms, where distances between merge points indicate similarity. Evaluated at all five k values.
- **GMM** (Gaussian Mixture Model): Probabilistic clustering assuming Gaussian component distributions. Parameters: `covariance_type='full', random_state=42`. Evaluated at all five k values.

This combination of unsupervised (2 configs) and supervised (10 configs: 5 hierarchical + 5 GMM) methods yields 12 clustering configurations per reduced embedding space.

3.4 | Evaluation metrics

During preliminary analysis, we computed several candidate metrics across all experimental configurations including: Adjusted Rand Index (ARI), Adjusted Mutual Information (AMI), Normalized Mutual Information (NMI), V-measure, homogeneity, completeness, purity, and silhouette score. After analyzing metric behavior across the full experimental space, we selected two complementary metrics as our primary evaluation framework to compare results, while including more evaluation metrics in the supplementary results and appendixes. The two complementary metrics selected for primary results are:

V-measure: The harmonic mean of homogeneity and completeness (detailed formulations in Appendix A). V-measure provides interpretable decomposition: homogeneity measures whether clusters contain only one species, while completeness measures whether species are split across clusters. This directly addresses ecological concerns about false grouping versus species fragmentation. Range: 0 to 1, where higher values indicate better clustering.

Adjusted Mutual Information (AMI): Information-theoretic agreement between predicted and ground truth partitions, adjusted for chance, see detailed formulations in Appendix A. AMI corrects for the bias that random clusterings achieve non-zero scores, making it critical when comparing methods with vastly different cluster counts, e.g., HDBSCAN finding 35 clusters vs. DBSCAN with 220 clusters. AMI serves as secondary validation, particularly for unsupervised methods. Range: 0 (random) to 1 (perfect), but can be negative when clustering performs worse than random.

Beyond quantitative metrics, we analyze cluster compositions to distinguish between true errors and biologically meaningful patterns. True errors include different species incorrectly grouped together (false positives) or same species incorrectly split without biological explanation (false negatives). However, some cluster splits may reveal fine-grained biological patterns which are manually inspected and documented. This analysis provides ecological value beyond pure species identification and informs when clustering can be trusted versus when expert validation remains essential.

The complete benchmarking code and the test results are released as open source (Section 6).

4 | RESULTS

Our testing compare experimental configurations across five ViT models, five dimensionality reduction methods, and four clustering algorithms with varying parameters, resulting in a total of 27,600 combinations. The summarized results with detailed performance matrices is provided in Appendix C, while the key-findings are described in the following sections. The most promising configurations are used to further test and evaluate performance on unevenly distributed data and intra-species specific findings.

4.1 | Vision transformer model performance

The selection of vision transformer model dramatically impacts clustering performance (Figure 5). Self-supervised DINO models substantially outperform the other vision-language models. DINOv3 achieves the highest average V-measure (0.817), followed by DINOv2 (0.769). In contrast, biology-specific BioCLIP 2 and general-purpose CLIP and SigLIP show substantially lower performance, with average V-measures ranging from 0.597 to 0.652. Notably, the distributions show consistent separation between models.

The performance advantage of DINO models extends across all dimensionality reduction and clustering method combinations. The complete result breakdown with additional performance metrics can be found in Appendix Table C5.

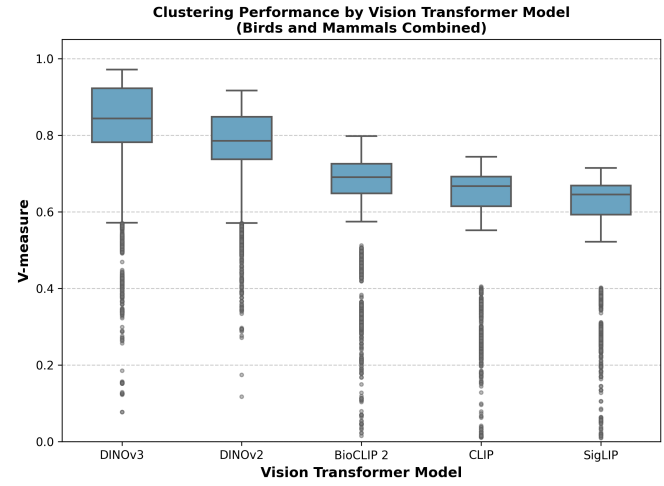


FIGURE 5 V-measure distribution across vision transformer models. Box plots show median, interquartile range, and outliers for all 5,520 configurations per model.

4.2 | Dimensionality reduction

Across all experimental configurations, t-SNE and UMAP consistently outperformed PCA, Isomap and Kernel PCA by 26–38 percentage points (Table 3, Figure 6). Not a single combination of PCA, Isomap or Kernel PCA achieved performance matching t-SNE or UMAP. Between the two best methods, t-SNE marginally outperforms UMAP by 0.6–1.1 percentage points on average, with smaller differences for birds (0.6 pp) than mammals (1.1 pp). However, the results reveal that UMAP performs slightly better in 23% of individual configurations, particularly with density-based clustering methods.

TABLE 3 Dimensionality Reduction Method Comparison

Method	Birds	Mammals	Average	Versus t-SNE
t-SNE	0.750	0.724	0.737	–
UMAP	0.744	0.713	0.729	-0.8 pp
Isomap	0.493	0.466	0.480	-25.7 pp
PCA	0.381	0.362	0.372	-36.5 pp
KPCA	0.382	0.325	0.354	-38.3 pp

V-Measure averaged across all experimental configurations for the different dimensionality reduction methods. pp = percentage points.

4.3 | Supervised clustering: hierarchical and GMM performance

When cluster count matches ground truth (K=30), Hierarchical clustering and Gaussian Mixture Models (GMM) achieve nearly identical performance across all model × dimensionality reduction combinations. Hierarchical clustering averages

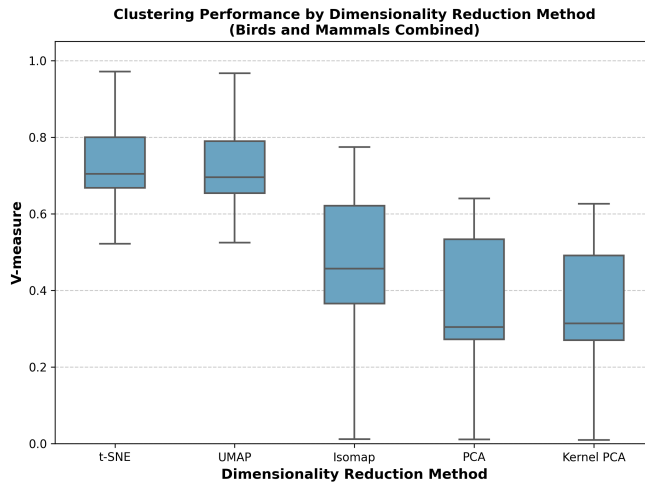


FIGURE 6 V-measure distribution across dimensionality reduction methods.

marginally higher (+0.001 to +0.006 V-measure difference), but this falls within variance bounds and individual runs show GMM occasionally outperforming Hierarchical.

The choice of K affects performance, with distinct patterns emerging between model classes. For DINOv3 and DINOv2, optimal performance occurs at the true species count (K=30), achieving average V-measures of 0.909 and 0.838 respectively in average across all the dimension reduction methods. These models maintain strong performance even under miscalculation: at K=45 (50% overestimate), DINOv3 retains 0.880 V-measure, representing only 3.2% degradation.

In contrast, the vision-language models BioCLIP 2, CLIP and SigLIP achieve better performance at K=45 rather than the true K=30. For these models, K=45 configurations yield 1–3% higher V-measures compared to K=30. The performance graph of the AMI and V-measure across the different K values and across all five ViT models can be seen in Figure 7.

For DINOv3 combined with the top performing dimension reduction methods, t-SNE and UMAP, the average V-measure averages at 0.960 for birds and 0.952 for mammals, using Hierarchical clustering with K=30 while GMM, K=30 reaching an average V-measure of 0.957 for birds and 0.952 for mammals. See Appendix Table C2.

4.4 | Unsupervised clustering: HDBSCAN VS DBSCAN

For real-world scenarios where species count is unknown, unsupervised methods must balance three criteria: (1) discovering the true count of clusters, (2) minimizing outliers requiring manual validation, and (3) achieving high clustering quality.

Our results demonstrate HDBSCAN dramatically outperforms DBSCAN across all three dimensions (Table 4).

Using the best-performing configuration (DINOv3 + t-SNE), we evaluate both methods:

- **Cluster count:** HDBSCAN produces cluster counts approximating ground truth (30 species), discovering on average 33 clusters for birds and 37 for mammals. In contrast, DBSCAN over-splits dramatically, producing 256 clusters for birds and 247 for mammals, representing 8× over-clustering.
- **Outlier ratio:** HDBSCAN classifies only 0.9% (birds) and 1.4% (mammals) of images as outliers requiring manual review. DBSCAN rejects 28–29% of samples across both taxonomic classes.
- **Clustering quality:** Despite operating without species count knowledge, HDBSCAN achieves V-measure of 0.948 (birds) and 0.939 (mammals), sacrificing only 1.3–1.5 percentage points compared to the supervised Hierarchical K=30 (V-measure = 0.961/0.954). DBSCAN achieves substantially lower V-measure of 0.668 for both classes.

This pattern persists across all model × dimensionality reduction combinations (Table C4), where DBSCAN consistently generates 150–260 clusters, while HDBSCAN maintains cluster counts within closer to ground truth.

Why DBSCAN fails: Automatic epsilon estimation, while theoretically sound, proves too sensitive to local density variations in the 2D embeddings, causing systematic over-fragmentation of species clusters.

TABLE 4 Unsupervised Clustering Performance Summary

Model	Dim. Red.	Clusters B/M	Outliers B/M	V-Measure B/M
<i>HDBSCAN Results</i>				
DINOv3	t-SNE	33/37	0.9%/1.4%	0.948/0.939
DINOv3	UMAP	47/57	4.2%/7.1%	0.917/0.890
DINOv2	t-SNE	34/45	2.3%/5.0%	0.903/0.843
DINOv2	UMAP	39/55	4.7%/8.3%	0.889/0.802
<i>DBSCAN Results</i>				
DINOv3	t-SNE	256/247	28%/29%	0.668/0.668
DINOv3	UMAP	204/189	31%/27%	0.674/0.687
DINOv2	t-SNE	221/218	28%/28%	0.677/0.672
DINOv2	UMAP	173/149	30%/26%	0.680/0.685

Averaged numbers. Ground truth: 30 clusters per class (B = Birds, M = Mammals)

4.5 | Consistent cluster count prediction

From our results, we found that combining DINOv3, t-SNE and HDBSCAN we were able to use unsupervised methods to find clusters with high homogeneity, while getting close to the ground truth number of clusters. We evaluated this

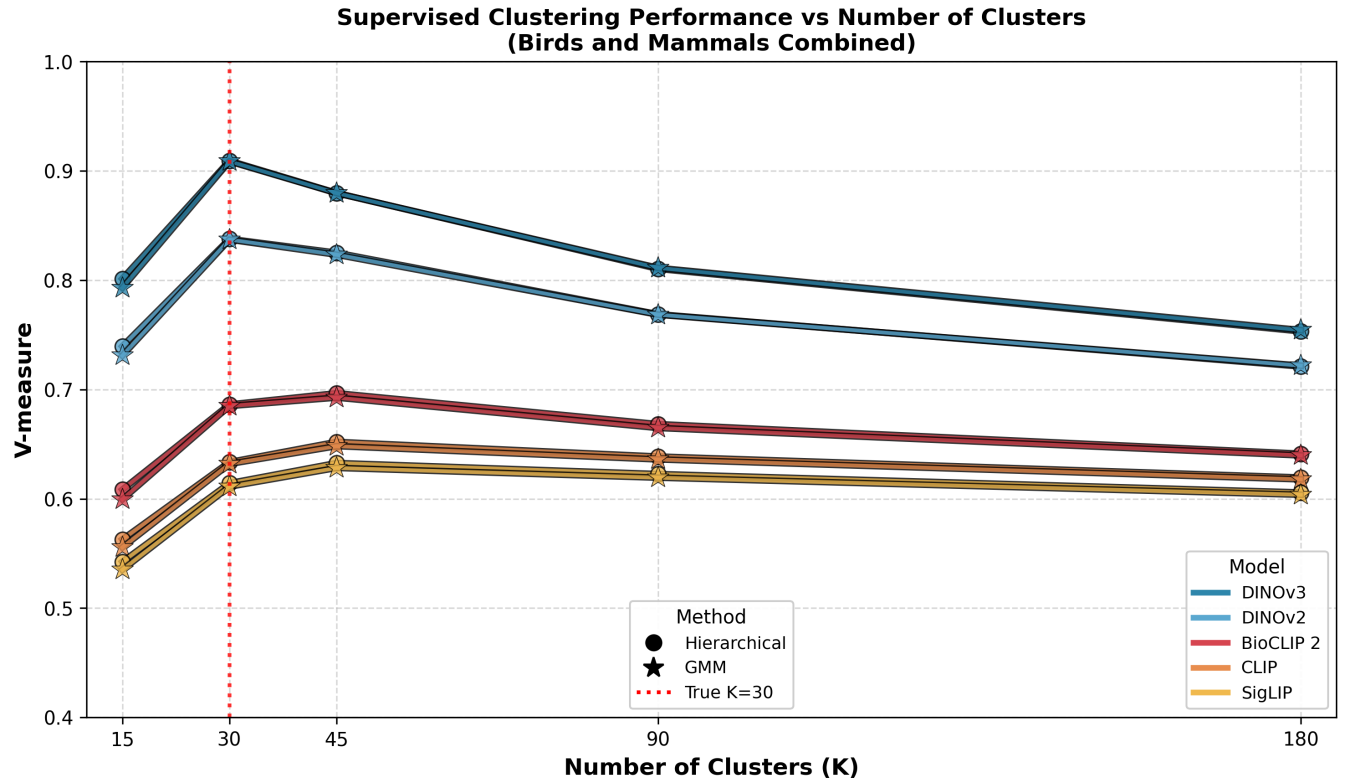


FIGURE 7 Average clustering performance (V-measure) as a function of the number of clusters K for five embedding models using hierarchical (circles) and GMM (stars) clustering. At the true number of species ($K = 30$, red dotted line), both clustering methods perform nearly identically. DINOv3 and DINOv2 achieve the highest scores and peak at $K = 30$. BioCLIP 2, CLIP and SigLIP instead peak at $K = 45$. See Table C3 for complete K -variation results across all models.

configuration's ability to predict the true cluster count by varying the number of species, $n \in \{5, 10, 15, 20, 25, 30\}$, for both birds and mammals. The selected species are randomized when $n < 30$, with 100 runs per n -value using identical pipeline settings (DINOv3 + t-SNE + HDBSCAN with `min_cluster_size=15, min_samples=5`), resulting in 1,200 total runs (600 for mammals and 600 for birds).

As shown in Figure 8, the predicted cluster count closely follows the ground truth across all values of n . At $n = 30$, the method predicts 33.5 ± 2.1 clusters for birds and 37.5 ± 2.9 clusters for mammals, representing a slight but consistent overestimation.

4.5.1 | Species-level clustering behavior

To understand clustering behavior at the species level, we introduce two complementary metrics. The *Isolation Index* (II) measures the average purity experienced by each image and

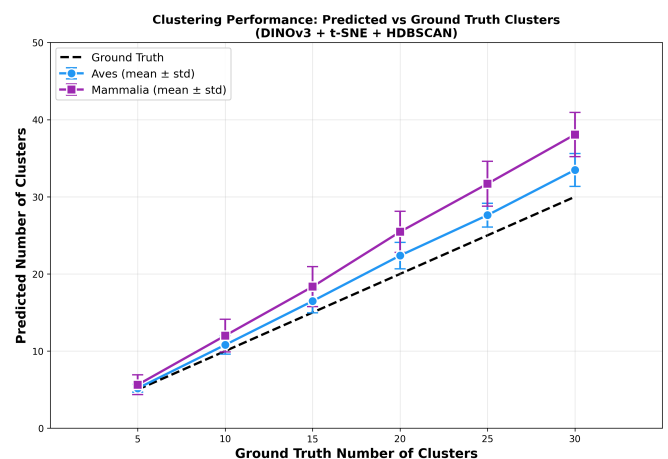


FIGURE 8 Mean predicted cluster count with standard deviation at different ground truth values $n \in \{5, 10, 15, 20, 25, 30\}$ for both mammals and birds, using DINOv3, t-SNE and HDBSCAN. The dashed line represents perfect prediction.

what fraction of its cluster-mates belong to the same species:

$$II_s = \frac{1}{N_s} \sum_{c \in C} \frac{n_{s,c}^2}{|cl|} \quad (1)$$

The *Effective Cluster Count* (ECC) measures how many clusters a species effectively “owns”:

$$ECC_s = \sum_{c \in C} \frac{n_{s,c}}{|cl|} \quad (2)$$

where N_s is the total number of images of species s , $n_{s,c}$ is the count of species s in cluster c , and $|cl|$ is the cluster size. Together, these metrics classify species into distinct behavioral categories (Table 5).

TABLE 5 Species clustering behavior at $n = 30$ using DINOv3 + t-SNE + HDBSCAN (100 runs). Species are grouped by behavior: **Oversplit** ($ECC \geq 1.5$, high II) fragment into multiple pure clusters; **Merged** ($II < 0.95$) share clusters with similar species; **Ideal** ($II \geq 0.95$, $ECC \approx 1$) form single pure clusters. M = Mammalia, A = Aves.

Species	II	ECC	Notes
<i>Oversplit — Multiple pure clusters</i>			
Least Weasel (M)	0.97	2.13	Seasonal pelage variation
Raccoon (M)	0.96	2.00	IR/RGB, posture variation
Red Junglefowl (A)	0.89	1.90	Sexual dimorphism
NZ Sea Lion (M)	0.95	1.84	Age/sex dimorphism
Pipit (A)	0.97	1.76	Cryptic plumage variation
Petrel (A)	0.91	1.71	Flight vs. ground poses
<i>Merged — Species pairs clustering together</i>			
Takahē (A)	0.58	0.83	↔ Swamphen
Swamphen (A)	0.58	0.99	↔ Takahē
Wolf (M)	0.63	1.78	↔ Jackal
Jackal (M)	0.64	1.47	↔ Wolf
Black Bear (M)	0.81	0.96	↔ Sun Bear
Sun Bear (M)	0.82	0.85	↔ Black Bear
<i>Ideal — Single pure cluster (ECC ≈ 1.0, II ≈ 1.0)</i>			
Gemsbok (M)	1.00	1.00	—
Porcupine (M)	1.00	1.00	—
Ostrich (A)	1.00	1.00	—
Kori Bustard (A)	1.00	1.00	—
+ 26 Ideal species omitted (16M, 10A)			

The results reveal three distinct clustering behaviors. **Oversplit** species fragment into multiple pure clusters due to high intra-specific variation: Least Weasel exhibits seasonal pelage changes (brown summer coat vs. white winter coat); Red Junglefowl shows strong sexual dimorphism between colorful males and cryptic females; NZ Sea Lion displays pronounced size dimorphism between sexes; Raccoon images split by imaging conditions (IR vs. RGB) and body postures. These splits,

while inflating cluster counts, do not compromise identification accuracy—each fragment remains species-pure and can be merged during post-processing.

Merged species pairs share clusters due to genuine visual similarity rather than model limitations: Wolf and Black-backed Jackal ($II \approx 0.63$) are both medium-sized canids with similar body proportions; Takahē and Australasian Swamphen ($II \approx 0.58$) are congeneric rails historically considered conspecific; Sun Bear shows the lowest ECC (0.85), indicating it is often absorbed into American Black Bear clusters rather than forming its own.

The majority of species (16/30 mammals, 14/30 birds) achieve **Ideal** clustering with $II \geq 0.95$ and ECC close to 1.0, demonstrating that the pipeline successfully isolates most species.

Notably, some species exhibit both behaviors simultaneously: Red Junglefowl has high $ECC = 1.90$ (oversplit) but also low $II = 0.89$ (merging with Chicken), indicating it forms multiple clusters while also sharing some with its domesticated descendant.

4.6 | Intra-specific variation and cluster splitting

To assess whether additional clusters (>30 per taxonomic class) could reveal ecologically meaningful intra-specific variation, we manually inspected clustering results from DINOv3 embeddings reduced via t-SNE and clustered using both DBSCAN and supervised methods with $K \in \{90, 180\}$. While supervised methods force all embeddings into clusters, DBSCAN produced smaller, more homogeneous sub-clusters that consistently captured the same traits across independent runs.

Manual inspection methodology: We selected the unsupervised clustering configurations that produced high over-splitting from our primary testing, combining DINOv3, t-SNE and DBSCAN. Using the same 10 image configurations for mammals and birds as used to create table C4, where DBSCAN created 224–278 bird clusters and 211–270 mammal clusters, which essentially means several smaller sub-clusters from each species. Then manually inspected the resulting sub-clusters. Since each subset was randomly sampled, trait prevalence varied, where some runs contained sufficient number of images to form distinct sub-clusters, while others did not. Clusters were tagged when a clear trait was identified where most tagged clusters were completely homogeneous, though a few contained minor outliers.

Observed intra-specific patterns: While manually inspecting clusters, we identified several intra-species traits, such as juvenile, sex, fur and feather coloration and patterns, and clusters collecting images of body parts, where the cropping only included e.g. feet of the animal, rather than the whole animal.

Additionally, we found clusters with different animal poses clustered together such as animals lying down. While looking for intra-species traits, we found clusters separating RGB, IR and white-light flash images across most species. At times, we also noticed clear patterns in clusters where the environmental background was dominant, such as clusters where snow was consistently present throughout.

We have selected a few species with observed traits, where we record the occurrence across 10 image runs and the results can be seen in Table 6. These traits and more, including more species, are available in the interactive web interface, provided as supplement to this paper (Section 6), where we aim to update and include more discoveries from the test data.

TABLE 6 Intra-specific variation detected via over-clustering (DINOv3 + t-SNE + DBSCAN). Fractions indicate runs where homogeneous trait clusters were identified.

Species	Trait Detected	Runs
Wolf	Juvenile individuals	10/10
	Dark/black fur phenotype	10/10
	IR (night) images	10/10
	Snow background context	10/10
Black-backed Jackal	Juvenile individuals	5/10
	IR (night) images	10/10
	White-light flash images	10/10
Dromedary Camel	Leg-only (partial body)	10/10
Greater Kudu	Males (IR images)	10/10
	Males (RGB images)	5/10
	Females + juveniles; lying posture	5/10
Kori Bustard	Juvenile individuals	5/10
Yellow-eyed Penguin	Juvenile individuals	10/10
Chicken	Feather pattern/color variants	10/10
	Males (sexual dimorphism)	3/10

These results demonstrate that vision transformer embeddings can capture fine-grained visual differences beyond species. Age classes (juveniles), sexual dimorphism (males vs. females), phenotypic variation (fur/feather color), imaging conditions (IR, flash and RGB), and environmental context (snow, posture) all produced separable clusters. We distinguish between two categories of detected patterns: biologically meaningful intra-specific variation and environmentally-driven clustering.

Intra-specific variation: Figures 9, 10, and 11 present representative examples of detected traits, with images sampled from homogeneous clusters identified across independent runs. Figure 9 shows two examples: (a) male Greater Kudu in IR images, distinguished by their spiral horns; and (b) juvenile Kori Bustards showing characteristic immature plumage. Additional wolf-specific examples, including dark fur phenotypes and juvenile individuals, are presented in Figure 10. While most clusters were highly homogeneous, occasional outliers may be present

where the embedding similarity was driven by other visual features. The consistency of these clusters across multiple random subsets suggests that the detected patterns reflect genuine visual structure in the embedding space rather than sampling artifacts.

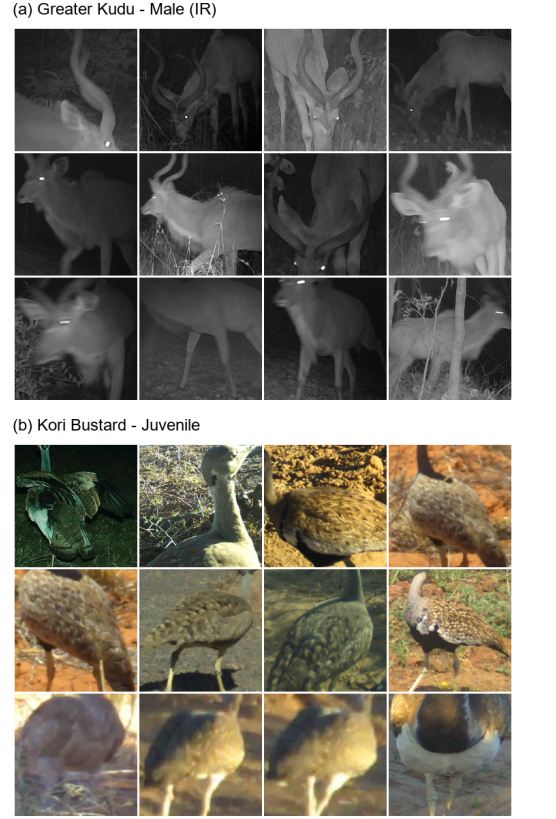


FIGURE 9 Examples of intra-specific variation detected via over-clustering (DINOv3 + t-SNE + DBSCAN). Each panel shows 12 images from a homogeneous cluster representing: (a) male Greater Kudu (IR); (b) juvenile Kori Bustards. Images were sampled from clusters identified across 10 independent runs with different random image subsets; occasional outliers may be present.

Environmental context clustering: Beyond biological traits, the embeddings also captured environmental and contextual features present in the images. Wolves photographed against snowy backgrounds were consistently grouped together across runs (see Figure 11, bottom panel). While such clusters do not represent intra-specific biological variation, they demonstrate the sensitivity of vision transformer embeddings to scene context and could be valuable for filtering images by environmental conditions or identifying seasonal patterns in camera trap data.

Location-agnostic clustering verification: A potential concern with camera trap datasets is that clustering might be driven by location-specific features, such as background vegetation,

camera angle, or lighting conditions, rather than biologically meaningful traits. To address this concern, we traced each wolf image back to its original camera trap location. The Idaho camera trap dataset includes location identifiers in the original filenames (e.g., **loc_0086**, **loc_0121**), enabling systematic verification of location diversity within each trait cluster.

Table 7 shows the number of unique camera locations contributing to each wolf trait cluster across 10 independent runs. The dark fur cluster contains images from 24 different camera locations across the study area, with individual runs clustering from 4–13 locations. Similarly, infrared night images span 55 unique locations, juvenile clusters span 16 locations, and snowy background images originate from 31 locations.

TABLE 7 Location distribution for wolf trait clusters across 10 independent runs. Each cell shows the number of unique camera locations contributing to that trait cluster.

Trait	R1	R2	R3	R4	R5	R6	R7	R8	R9	R10
Dark Fur	6	13	7	5	4	11	9	11	8	10
Juvenile	8	4	6	2	2	3	5	5	5	5
Night Images (IR)	15	16	16	19	23	19	22	23	30	29
Snowy Background	9	9	7	8	8	13	10	17	12	13

Figures 10 and 11 present representative examples from each wolf trait cluster from run 1 (R1), where each of the six images originates from a different camera trap location. The visual coherence within each panel, despite the diverse geographic origins, demonstrates that DINOv3 embeddings capture genuine phenotypic and contextual patterns rather than location-specific artifacts.

4.7 | Performance on unevenly distributed data

While our initial tests used 200 images per species, real-world camera-trap deployments typically exhibit long-tailed species distributions where common species vastly outnumber rare ones. We systematically evaluated whether this imbalance affects clustering quality.

We compared the original HDBSCAN(15,5) configuration, combined with DINOv3 and t-SNE, across three distribution scenarios: even (200 images/species), mild imbalance (20–200 images/species), and extreme variation reflecting realistic deployment conditions (Table 8). The extreme scenario samples randomly between 20 and the maximum available images per species, resulting in ranges of 48–4,145 for Aves and 29–6,431 for Mammalia.

The mild imbalance (20–200 images per species) shows *no degradation*, in fact, cluster estimation slightly improves. However, extreme imbalance causes significant over-clustering:

TABLE 8 Effect of sample distribution on clustering with 30 species (DINOv3 + t-SNE). *Even*: 200 img/sp. *Uneven*: 20–200 img/sp. *Extreme*: random 20–max img/sp.

Method	Aves		Mammalia	
	V-measure	Clusters	V-measure	Clusters
HDBSCAN(15,5)				
Even	0.948±0.006	33±3	0.939±0.006	37±3
Uneven	0.954±0.006	31±1	0.950±0.009	33±2
Extreme	0.776±0.029	415±92	0.792±0.022	304±51

HDBSCAN produced an average of 415 clusters for Aves and 304 for Mammalia instead of the target 30, representing 10–14× over-clustering. While homogeneity remains high under extreme imbalance (see Appendix Table D6), this comes at the cost of substantially more outliers and fragmented clusters requiring manual review.

4.7.1 | Parameter optimization for extreme imbalance

To address the over-clustering issue, we tested configurations with larger `min_cluster_size` values for HDBSCAN and larger `min_samples/epsilon` multipliers for DBSCAN (see Appendix D for comprehensive results across 20 configurations). Table 9 summarizes the two best-performing configurations for each clustering method, including results on combined bird and mammal data.

TABLE 9 Best configurations for extreme uneven distributions (20–MAX images per species). Results averaged over 10 different image distributions. Full results in Appendix Table D6.

Config	t-SNE			UMAP		
	V-m	Cl.	O%	V-m	Cl.	O%
<i>Aves (30 species)</i>						
HDBSCAN(100,30)	0.936	43	4.7	0.922	45	3.0
HDBSCAN(150,50)	0.946	36	4.7	0.933	36	2.3
DBSCAN(1.5,20)	0.909	75	2.3	0.910	80	2.9
DBSCAN(2.0,30)	0.911	28	0.3	0.940	45	1.6
<i>Mammalia (30 species)</i>						
HDBSCAN(100,30)	0.918	44	3.9	0.920	45	2.1
HDBSCAN(150,50)	0.930	39	3.7	0.926	40	1.9
DBSCAN(1.5,20)	0.887	68	2.1	0.877	85	3.9
DBSCAN(2.0,30)	0.899	32	0.2	0.914	50	1.1
<i>Combined (60 species)</i>						
HDBSCAN(100,30)	0.936	91	4.2	0.933	89	3.1
HDBSCAN(150,50)	0.948	72	4.1	0.942	74	2.3
DBSCAN(1.5,20)	0.900	167	2.8	0.910	155	4.3
DBSCAN(2.0,30)	0.930	68	0.5	0.939	95	1.6

V-m=V-measure, Cl.=Clusters found (true: 30/30/60), O%=Outlier ratio.

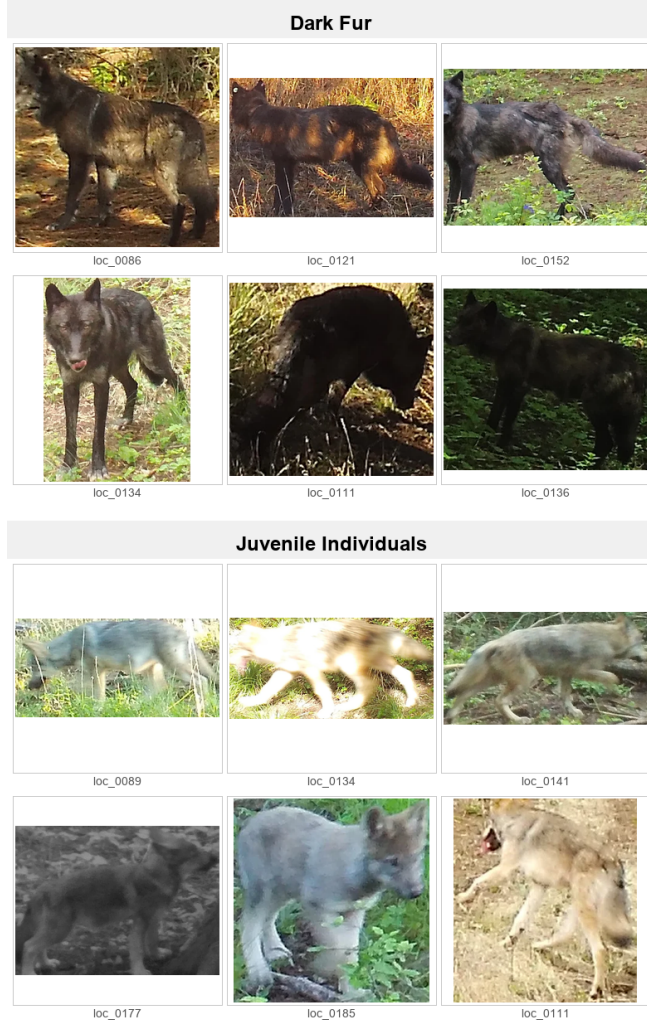


FIGURE 10 Location-agnostic clustering of biological traits. Samples from clusters of a single run (R1).

When balancing V-measure, cluster count accuracy, and outlier rates, HDBSCAN(150,50) emerged as the most effective configuration for extreme uneven distributions, achieving $V=0.948$ with t-SNE and $V=0.942$ with UMAP on the combined 60-species dataset. The DBSCAN(2.0,30) configuration also performs well with the lowest outlier rate (0.5% for t-SNE), though it occasionally produces fewer clusters than the true species count.

4.7.2 | Scaling behavior

To further evaluate the scalability of the configurations optimized for extreme imbalance, we tested them across varying numbers of species: $n = 5, 10, \dots, 30$ for single-class datasets and $n = 5, 10, \dots, 60$ for combined datasets. Each test used 10 random species samples with 20-MAX images per species.

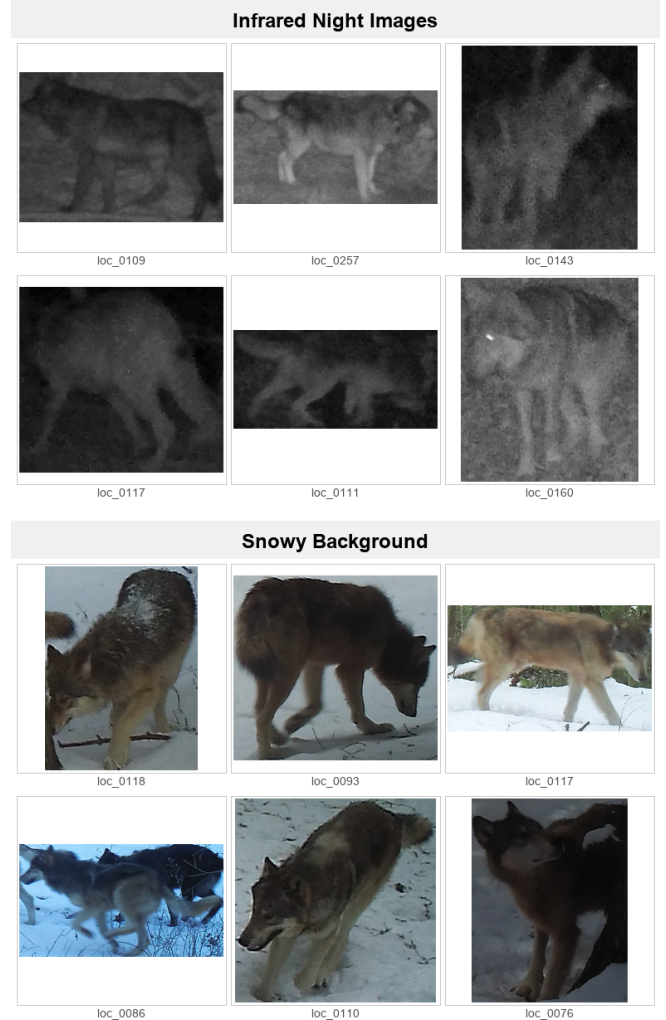


FIGURE 11 Location-agnostic clustering of IR images and images with snowy backgrounds with wolves. Samples from clusters of a single run (R1).

Both HDBSCAN configurations showed minimal scaling degradation, maintaining V-measure above 0.92 and closely tracking the true species count across all tested values (Figure 12). The two DBSCAN configurations exhibited scaling limitations. DBSCAN(1.5,20) achieved comparable homogeneity to the HDBSCAN configurations but consistently over-clustered, reducing V-measure. DBSCAN(2.0,30) showed promising results with UMAP but tended to under-cluster with t-SNE, lowering homogeneity.

4.7.3 | Generalization across distribution types

To verify that optimized configurations generalize beyond their tuning scenario, we applied all methods to both even and extreme distributions (Table 10).

Scaling Behavior: t-SNE with Combined Birds and Mammals

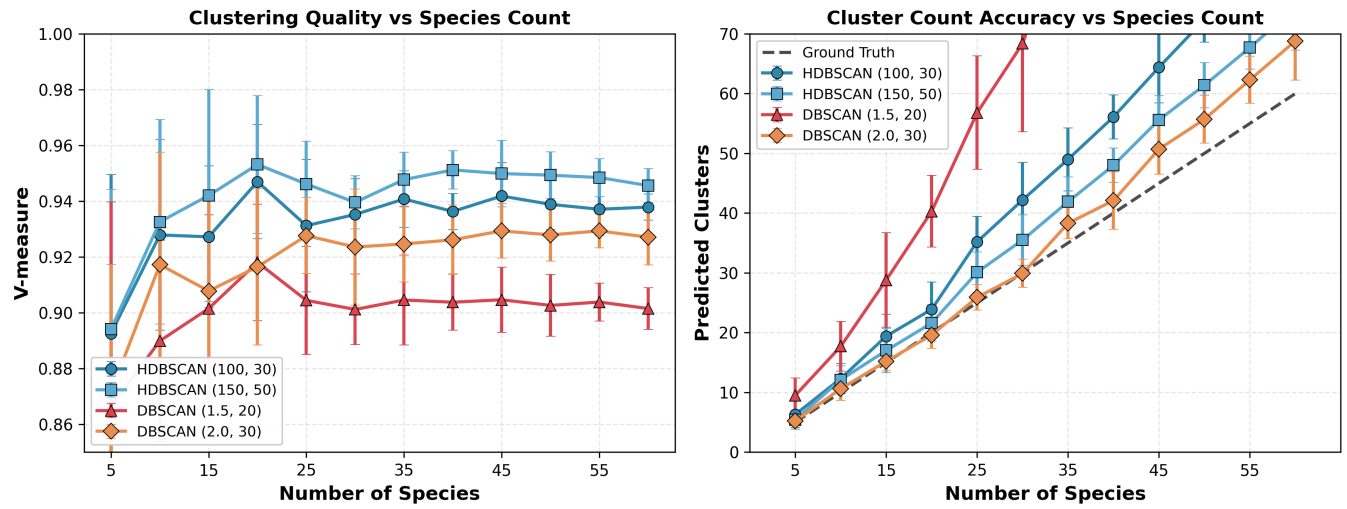


FIGURE 12 Scaling behavior of unsupervised clustering using t-SNE on combined bird and mammal datasets (DINOv3 embeddings). Left: V-measure remains high (> 0.92) as species count increases from 5 to 60. Right: Predicted cluster count closely tracks ground truth (dashed line) across all configurations. Error bars show standard deviation across 10 experimental runs. See Figure D1 in Appendix D for complete results across the selected configurations.

TABLE 10 Clustering performance across distribution types (DINOv3 + t-SNE, 30 species). *Even*: 200 img/sp. *Extreme*: 20-max img/sp.

Method	Aves			Mammalia		
	V-m	Cl.	O%	V-m	Cl.	O%
<i>HDBSCAN(15,5) – Original</i>						
Even	0.948 \pm 0.006	33 \pm 3	0.9	0.939 \pm 0.006	37 \pm 3	1.4
Extreme	0.776 \pm 0.029	415\pm92	14.2	0.792 \pm 0.022	304\pm51	12.2
<i>HDBSCAN(100,30) – Optimized</i>						
Even	0.951 \pm 0.007	29 \pm 2	1.1	0.947 \pm 0.004	29 \pm 2	1.9
Extreme	0.936 \pm 0.012	43 \pm 4	4.7	0.918 \pm 0.015	44 \pm 3	3.9
<i>HDBSCAN(150,50) – Optimized</i>						
Even	0.943 \pm 0.009	27 \pm 2	1.2	0.926 \pm 0.019	26 \pm 3	1.6
Extreme	0.946 \pm 0.009	36 \pm 3	4.7	0.930 \pm 0.015	39 \pm 3	3.7
<i>DBSCAN(1.5,20) – Optimized for Extreme</i>						
Even	0.324	41	77.6	0.324	41	77.6
Extreme	0.909	75	2.3	0.887	68	2.1
<i>DBSCAN(2.0,30) – Optimized for Extreme</i>						
Even	0.383	34	72.5	0.383	34	72.5
Extreme	0.911	28	0.3	0.899	32	0.2

V-m=V-measure, Cl.=Clusters found (target: 30), O%=Outlier ratio. Bold indicates problematic values.

DBSCAN configurations optimized for extreme imbalance fail on evenly distributed data, with 72–78% of images classified as outliers. This occurs because the larger epsilon multipliers tuned for the spread-out extreme distributions over-smooth the denser, more uniform clusters in even data, causing most points to fall outside cluster boundaries.

In contrast, both optimized HDBSCAN configurations demonstrate robust performance across distribution types.

HDBSCAN(100,30) achieves V-measure of 0.947–0.951 on even data while maintaining 0.918–0.936 on extreme distributions. HDBSCAN(150,50) shows remarkable consistency, actually performing *better* on extreme Aves data (V=0.946) than on even data (V=0.943), while keeping outlier rates below 5%.

This asymmetry has important practical implications: HDBSCAN configurations can be safely applied without prior knowledge of data distribution, whereas DBSCAN requires distribution-specific tuning and should be avoided when distribution characteristics are unknown.

Understanding the HDBSCAN parameters: `min_cluster_size` specifies the minimum number of images required to form a cluster. With HDBSCAN(150,50), species having fewer than 150 images cannot form their own cluster and will either be merged into a visually similar larger cluster or become outliers requiring manual review.

4.7.4 | Fate of under-represented species

A critical question for practical deployment is what happens to species with fewer images than the `min_cluster_size` threshold. We tracked outcomes for all such species across our scaling experiments (Table 11).

The choice of dimensionality reduction significantly affects how under-represented species are handled. With t-SNE, approximately 60–74% of under-threshold species become outliers, while 26–41% merge into larger clusters. UMAP

TABLE 11 Fate of species with fewer images than `min_cluster_size` threshold. Shows percentage classified as outliers vs merged into other clusters.

Method	Dataset	HDBSCAN(100,30)		HDBSCAN(150,50)	
		Outlier	Merged	Outlier	Merged
t-SNE	Aves	71%	29%	70%	30%
t-SNE	Mammalia	69%	31%	74%	26%
t-SNE	Combined	59%	41%	60%	40%
UMAP	Aves	22%	78%	37%	63%
UMAP	Mammalia	60%	40%	48%	52%
UMAP	Combined	37%	63%	41%	59%

shows the opposite pattern: only 22–48% become outliers, with 52–78% merging into visually similar clusters.

This difference has practical implications for workflow design. If the goal is to flag rare species for expert review, t-SNE’s higher outlier rate is advantageous, rare species are more likely to appear in the outlier pool requiring manual inspection. If the goal is to minimize data requiring manual attention (accepting that rare species may be grouped with visually similar species), UMAP’s tendency to merge is preferable. In both cases, the optimized configurations maintain high overall V-measure (>0.92) while providing interpretable behavior for edge cases.

4.7.5 | Practical recommendations

Our results demonstrate that DINOv3 combined with t-SNE and HDBSCAN provides robust species-level clustering across distribution types, with UMAP offering a viable alternative with lower outlier rates. The ideal deployment produces high-homogeneity clusters approximating the true species count, with outliers capturing rare species and ambiguous images for targeted manual inspection.

Parameter selection should be guided by expected data characteristics:

- **Large datasets (>1000 images, >150 images per expected species):** HDBSCAN(150,50) provides optimal balance of cluster purity, accurate cluster count estimation, and manageable outlier rates (3–5%).
- **Moderate datasets or mixed representation:** HDBSCAN(100,30) offers a middle ground, maintaining strong performance on both even and uneven distributions.
- **Smaller datasets or expected rare species (<100 images for some species):** The original HDBSCAN(15,5) configuration prevents rare species from being systematically excluded from clustering, though at the cost of potential over-clustering with extreme imbalance.
- **Prioritizing rare species detection:** Combine t-SNE with higher `min_cluster_size` to maximize the proportion

of under-represented species classified as outliers for expert review.

DBSCAN configurations, while effective when tuned for specific distributions, should be avoided when distribution characteristics are unknown or variable, as they fail to generalize across distribution types.

4.8 | Effect of dimensionality

We conducted testing comparing clustering directly on raw high-dimensional embeddings (768D–1536D) against 2D t-SNE-reduced spaces (Table 12). Dimensionality reduction consistently improved clustering performance across all models and methods.

For HDBSCAN, t-SNE reduction improved the mean V-measure from 0.498 (raw) to 0.783, an absolute gain of 0.285. Vision-language models benefited most dramatically: CLIP improved from 0.212 to 0.697, and SigLIP from 0.196 to 0.671. DINO models showed smaller but consistent improvements (DINOv3: 0.819 to 0.943).

For Hierarchical clustering at $K=30$, t-SNE reduction improved the mean V-measure from 0.432 to 0.784, an absolute gain of 0.352. However, this comparison is affected by algorithm failures: Hierarchical clustering failed entirely on raw high-dimensional DINOv2 and BioCLIP2 embeddings due to covariance matrix singularity, but worked reliably on all t-SNE-reduced embeddings.

DBSCAN exhibited opposite behavior, performing better on raw embeddings (DINOv3: mean of 38 clusters with V-measure of 0.693) while severely over-clustering with t-SNE (mean of 251 clusters with V-measure of 0.668), suggesting the automatic epsilon estimation is more stable in high-dimensional spaces where density variations are less pronounced.

5 | DISCUSSION

5.1 | Reduction to higher dimensions

Throughout our tests, we either kept the raw embedding dimensions (768D–1536D depending on model architecture) or reduced them drastically to a 2D space. This reduction discards substantial information encoded in the original embeddings. While 2D projections are great for visualization and manual cluster inspection, they may not be optimal for clustering performance.

Intermediate dimensionalities such as 32D, 64D, 128D, or 256D could potentially offer a better trade-off between information preservation and computational tractability. Such

TABLE 12 Effect of dimensionality on clustering performance. Comparison of clustering directly on raw high-dimensional embeddings versus t-SNE-reduced embeddings (2D). V-measure reported as mean across 10 Aves and 10 Mammalia subsamples. Values of 0.000 indicate algorithm failure due to covariance matrix singularity.

Model	Dim.	HDBSCAN		Hierarchical (K=30)	
		Raw	t-SNE	Raw	t-SNE
DINOv3	1280D	0.819	0.943	0.920	0.958
DINOv2	1536D	0.745	0.873	0.000 [†]	0.879
BioCLIP2	768D	0.519	0.730	0.000 [†]	0.737
CLIP	768D	0.212	0.697	0.629	0.688
SigLIP	768D	0.196	0.671	0.611	0.661
Mean	—	0.498	0.783	0.432*	0.784

[†]Algorithm failed due to covariance matrix singularity.

*Mean excludes failed runs (DINOv2, BioCLIP2).

representations would retain more of the semantic structure captured by the vision transformers while still reducing noise.

An approach combining higher-dimensional reduction for clustering with subsequent 2D projection for visualization could potentially improve clustering accuracy while maintaining interpretability. This would decouple the optimization objectives: preserving cluster-relevant structure in the higher-dimensional space while using 2D solely for human inspection of results. Future work could systematically evaluate clustering performance across a range of target dimensionalities to identify optimal configurations for different taxonomic groups and dataset sizes.

5.2 | Configuration importance

Our results demonstrate that clustering algorithm performance is parameter-dependent, and optimal configurations vary with data characteristics. While HDBSCAN consistently outperformed DBSCAN across our benchmark, this finding is contingent on parameter selection.

Our systematic evaluation of parameter configurations (Table D6) revealed that the original HDBSCAN(15,5) configuration, while optimal for evenly distributed data (V-measure = 0.943), fails dramatically on extreme uneven distributions, producing 300–400 clusters instead of the target 30. Conversely, configurations optimized for imbalanced data—HDBSCAN(100,30) and HDBSCAN(150,50), generalize well to both distribution types, maintaining V-measure >0.92 across scenarios.

DBSCAN exhibited more severe sensitivity: configurations tuned for extreme imbalance classified 72–78% of images as outliers when applied to evenly distributed data (Table 10). This asymmetry has critical practical implications: HDBSCAN

parameters can be selected conservatively for unknown distributions, whereas DBSCAN requires distribution-specific tuning and should be avoided when data characteristics are uncertain.

We recommend practitioners: (1) use HDBSCAN over DBSCAN for robustness to unknown distributions; (2) set `min_cluster_size` based on the minimum expected images per species, HDBSCAN(150,50) for large datasets, HDBSCAN(100,30) for moderate ones; and (3) validate parameter choices on subsets when possible before full deployment.

5.3 | Clustering failure analysis

Our quantitative analysis of species-level clustering behavior (Table 5) reveals systematic failure patterns that reflect genuine visual similarity rather than model limitations. Species pairs with low Isolation Index ($II < 0.70$) consistently share taxonomic or morphological similarity: Wolf and Black-backed Jackal ($II \approx 0.63$) are both medium-sized canids with similar body proportions; Takahē and Australasian Swamphen ($II \approx 0.58$) are congeneric rails historically considered conspecific; American Black Bear and Sun Bear ($II \approx 0.81$) share ursid body morphology despite geographic separation.

These merging failures are exacerbated by imaging conditions. IR (infrared) images, which lack color information and often capture animals at distance, showed particularly high inter-species confusion. Night images of canids, for instance, reduced distinguishing features to silhouette and relative size, features that overlap substantially between wolves and jackals. Similarly, black-feathered bird species showed elevated confusion rates in low-light conditions where plumage details were obscured.

DINOv3 embeddings generally achieved better species separation than other models, but imperfect separation persists for visually similar taxa. Notably, the embedding space retains meaningful structure even within merged clusters. We observed that images of different species within a shared cluster tend to occupy distinct sub-regions, with species boundaries often visible along embedding coordinate gradients. This suggests a practical workflow enhancement: rather than presenting merged cluster images in random order for manual review, sorting by embedding coordinates (x/y position in 2D space) can facilitate faster species separation by grouping visually similar images together. While manual validation remains necessary for merged clusters, coordinate-based sorting reduces workload by exploiting the partial separation preserved in the embedding geometry.

Oversplit species ($ECC > 1.5$) present a different challenge. Species like Least Weasel ($ECC = 2.13$) and Raccoon ($ECC = 2.00$) fragment into multiple pure clusters, likely reflecting high intra-specific variation in pelage, posture, or imaging conditions. These splits, while inflating cluster counts, do not

compromise identification accuracy, each fragment remains species-pure and can be merged during post-processing.

5.4 | Spatial organization patterns

For the two DINO models and BioCLIP 2, on evenly distributed species data, using t-SNE, we noticed from the 2D plots that clusters with high heterogeneity were often closer to the center of the plot, while more homogeneous clusters were located further away from the center. The high homogeneity clusters often visually separated further away from the center, and clustered more densely. This information could be used to further evaluate the likelihood of how well the clusters are homogeneous: the further away the cluster are from (x=0, y=0) the higher likelihood the cluster is homogeneous.

5.5 | Broader applicability and future directions

While this study focused on birds and mammals, we hypothesize that zero-shot clustering generalizes to other taxonomic groups. Camera trap and underwater monitoring systems increasingly target fishes, insects, reptiles and amphibians, all of which present similar challenges of high image volume and limited annotation capacity. Detection models similar to MegaDetector already exist for fish (Community Fish Detector) and insects (FlatBug), enabling the same crop-then-cluster pipeline evaluated here. The self-supervised nature of DINOv3 embeddings, trained on general visual features rather than taxon-specific datasets, suggests broad applicability, though performance may vary with morphological distinctiveness and imaging conditions specific to each domain.

A key direction for future work is systematically separating biological traits from environmental factors within the embedding space. Our results (Table 6) show that DINOv3 captures both types of variation, which is valuable for ecologists, that may want to filter by imaging conditions or analyze population demographics depending on their research goals.

Additionally, hierarchical clustering approaches that first separate species, then systematically subdivide clusters to reveal intra-specific structure, could provide ecologists with multi-resolution views of their data. Such workflows would enable both rapid species-level sorting and detailed population demographic analysis from the same embedding space, maximizing the utility of foundation model representations for biodiversity monitoring.

6 | OPEN-SOURCE CONTRIBUTIONS

Together with the publication of this paper, we release the full dataset of 139,111 annotated cropped images, together with an interactive demo to visualize some combinations of the different methods used, to visualize the 2D space the embedding points and the corresponding clusters and images. We also release benchmarking code in GitHub for anyone to reproduce and test the experiments we conducted, while giving the possibility to run the same tests with other ViT models and other types of data. Finally, we give access to all the collected logs and configurations tested used in this paper. All the contributions can be found in https://hugomarkoff.github.io/animal_visual_transformer/

7 | CONCLUSION

This study addressed a fundamental challenge in biodiversity monitoring: whether Vision Transformer foundation models can reduce manual annotation burden by automatically clustering unlabeled camera trap images into species-level groups. Through systematic evaluation of 27,600 experimental configurations across 60 species and 139,111 validated images, we demonstrate that zero-shot clustering provides a practical pathway to accelerate ecological image analysis workflows.

Our benchmarking reveals that model selection has the greatest impact on clustering performance. Self-supervised DINOv3 achieves near-perfect species-level clustering with a V-measure of 0.958, substantially outperforming biology-specific BioCLIP 2 at 0.737 and general-purpose vision-language models such as CLIP and SigLIP. This result suggests that self-supervised learning on diverse visual data produces more transferable representations than the domain-specific training for clustering tasks. Dimensionality reduction proves essential, with t-SNE and UMAP improving clustering performance by 26–38 percentage points compared to other tested methods. For practical deployment where species counts are unknown, unsupervised HDBSCAN clustering achieves competitive performance with a V-measure of 0.943 while discovering cluster counts within 18% of ground truth and rejecting only 1.14% of images as outliers requiring expert review.

Beyond quantitative metrics, our ecological interpretation reveals that clustering failures often encode meaningful biological structure. Species pairs that cluster together, such as Wolf and Black-backed Jackal or Takahē and Australasian Swamphen, share genuine morphological or taxonomic similarity rather than representing model limitations. Conversely, over-split species consistently separate by age classes, sexual

dimorphism, pelage variation, and environmental context, patterns valuable for population demographic analysis that would otherwise require manual annotation.

Our evaluation of a long-tailed distribution of species demonstrates that optimized HDBSCAN configurations maintain V-measure above 0.92 across both balanced and extremely imbalanced data typical of field deployments. This robustness, combined with the interpretable behavior of rare species appearing either as outliers for expert review or merging with visually similar taxa, makes the approach practical for real-world camera trap workflows.

Our evaluation focused on mammals and birds from camera trap imagery, and performance may differ for taxonomic groups with lower morphological distinctiveness or imaging modalities. Additionally, our 2D reduction approach, while enabling visualization and effective clustering, may discard information that higher-dimensional representations would preserve.

Future work should extend evaluation to additional taxonomic groups including fishes, insects, and reptiles where detection models already exist. Systematic testing of intermediate dimensionalities between 32D and 256D could optimize the trade-off between information preservation and clustering performance. Hierarchical clustering workflows that first separate species and then systematically reveal intra-specific structure would provide ecologists with multi-resolution views of their data.

Zero-shot clustering fundamentally transforms the annotation task from exhaustive image-by-image labeling to targeted review of cluster compositions. As camera trap networks expand globally and autonomous monitoring systems generate unprecedented image volumes, methods that organize unlabeled data before expert intervention become essential infrastructure for timely conservation decision-making. Our open-source toolkit, validated dataset, and comprehensive benchmarking results provide a foundation for continued development of zero-shot approaches in biodiversity monitoring.

REFERENCES

(2024) *Desert lion conservation camera traps*. LILA BC, <https://lila.science/datasets/desert-lion-conservation-camera-traps>.

(2024) *Island conservation camera traps*. LILA BC, <https://lila.science/datasets/island-conservation-camera-traps>.

(2024) *Snapshot camdeboo camera trap images*. LILA BC, <https://lila.science/datasets/snapshot-camdeboo>.

(2024) *Snapshot enonkishu camera trap images*. LILA BC, <https://lila.science/datasets/snapshot-enonkishu>.

(2024) *Snapshot karoo camera trap images*. LILA BC, <https://lila.science/datasets/snapshot-karoo>.

(2024) *Snapshot kgalagadi camera trap images*. LILA BC, <https://lila.science/datasets/snapshot-kgalagadi>.

(2024) *Snapshot kruger camera trap images*. LILA BC, <https://lila.science/datasets/snapshot-kruger>.

(2024) *Snapshot mountain zebra camera trap images*. LILA BC, <https://lila.science/datasets/snapshot-mountain-zebra>.

(2024) *Snapshot safari 2024 expansion*. LILA BC, <https://lila.science/datasets/snapshot-safari-2024-expansion>.

(2024) *Trail camera images of New Zealand animals*. LILA BC, <https://lila.science/datasets/nz-trailcams>.

(2024) *UNSW predators camera traps*. LILA BC, <https://lila.science/datasets/unsw-predators>.

Abboud, A., Cohen-Addad, V. & Houdrouge, H. Subquadratic high-dimensional hierarchical clustering. In: *Proc. 33rd Conf. Neural Information Processing Systems (NeurIPS)*, 2019.

Anton, V., Hartley, S., Geldenhuys, A. & Wittmer, H.U. (2018) Monitoring the mammalian fauna of urban areas using remote cameras and citizen science. *J. Urban Ecol.*, 4(1).

Appel, C.L. et al. (2025) Developing custom computer vision models with Njobvu-AI: A collaborative, user-friendly platform for ecological research. *Ecol. Appl.*, 35(6), e70096.

Balasubramaniam, S. (2024) Optimized classification in camera trap images: An approach with smart camera traps, machine learning, and human inference. Master's thesis, The Ohio State University.

Becht, E. et al. (2019) Dimensionality reduction for visualizing single-cell data using UMAP. *Nature Biotechnology*, 37(1), 38–44.

Beery, S., Morris, D. & Yang, S. (2019) *Efficient pipeline for camera trap image review*. ArXiv:1907.06772.

Beery, S., Van Horn, G. & Perona, P. Recognition in terra incognita. In: *Proc. 15th European Conf. Computer Vision (ECCV)*, 2018a.

Beery, S., Van Horn, G. & Perona, P. Recognition in terra incognita: Using domain adaptation to improve wildlife classification for new camera trap locations. In: *Proc. ECCV*, 2018b, pp. 456–473.

Campello, R.J.G.B., Moulavi, D. & Sander, J. Density-based clustering based on hierarchical density estimates. In: *Pacific-Asia Conference on Knowledge Discovery and Data Mining*, 2013. : Springer, pp. 160–172.

Dosovitskiy, A. et al. An image is worth 16x16 words: Transformers for image recognition at scale. In: *Proc. ICLR*, 2021.

Gadot, T., Istrate, S., Kim, H., Morris, D., Beery, S., Birch, T. et al. (2024) *SpeciesNet: Animal classification model*. <https://doi.org/10.1049/cvi2.12318>.

Gadot, T., Istrate, S., Kim, H., Morris, D., Beery, S., Birch, T. et al. (2024) To crop or not to crop: Comparing whole-image and cropped classification on a large dataset of camera trap images. *IET Computer Vision*, 18(8), 1193–1208. Doi: 10.1049/cvi2.12318.

Gu, J. et al. (2025) *BioCLIP 2: Emergent properties from scaling hierarchical contrastive learning*. ArXiv:2505.23883.

Idaho Dep. of Fish and Game (2024) *Idaho camera traps*. LILA BC, <https://lila.science/datasets/idaho-camera-traps>.

Kobak, D. & Berens, P. (2019) The art of using t-SNE for single-cell transcriptomics. *Nature Communications*, 10(1), 5416.

LILA (2018) *LILA BC datasets*. <https://lila.science/datasets>.

Lowe, A. & Haurum, J.B. (2024) *Zero-shot clustering of ecological image embeddings using ViT models*. OpenReview.

Markoff, H. & Galaktionovs, J. (2025) *Animal detect: Camera trap image processing platform*. <https://www.animaldetect.com/>.

Markoff, H. & Galaktionovs, J. (2025) *Hierarchical re-classification: Combining animal classification models with vision transformers*. ArXiv:2510.14594.

McInnes, L., Healy, J. & Melville, J. (2018) *UMAP: Uniform manifold approximation and projection for dimension reduction*. ArXiv:1802.03426.

Morris, D. (2024) *Seattle(ish) camera traps*. LILA BC, <https://lila.science/datasets/seattleish-camera-traps>.

Norouzzadeh, M.S. et al. (2021) A deep active learning system for species identification and counting in camera trap images. *Methods in Ecology and Evolution*, 12(1), 150–161.

Oquab, M., Dariset, T., Moutakanni, T., Vo, H.V., Szafraniec, M., Khalidov, V. et al. (2023) *DINOv2: Learning robust visual features without supervision*. ArXiv:2304.07193.

Pantazis, O. et al. Focus on the positives: Self-supervised learning for biodiversity monitoring. In: *Proc. ICCV*, 2021, pp. 10582–10592.

Radford, A. et al. Learning transferable visual models from natural language supervision. In: *Proc. ICML*, 2021, pp. 8748–8763.

Reynolds, D. (2009) Gaussian mixture models. In: *Encyclopedia of Biometrics*. Vol. 741pp. 659–663.

Rigoudy, N., Dussert, G., Benyoub, A. et al. (2023) The DeepFaune initiative: a collaborative effort towards the automatic identification of European fauna in camera trap images. *European Journal of Wildlife Research*, 69, 113. Doi: 10.1007/s10344-023-01742-7.

Siméoni, O., Vo, H.V., Seitzer, M., Baldassarre, F., Oquab, M., Jose, C. et al. (2025) *DINOv3*. ArXiv:2508.10104.

Stevens, S. et al. BioCLIP: A vision foundation model for the tree of life. In: *Proc. CVPR, 2024*, pp. 19412–19424.

Svenning, A. et al. (2025) A general method for detection and segmentation of terrestrial arthropods in images. bioRxiv, doi: 10.1101/2025.04.08.647223.

Swanson, A.B., Kosmala, M., Lintott, C.J., Simpson, R.J., Smith, A. & Packer, C. (2015) Snapshot serengeti, high-frequency annotated camera trap images of 40 mammalian species in an African savanna. *Scientific Data*, 2, 150026.

SWG (2021) *Northern and central annamites camera traps 2.0*. LILA BC, <https://lila.science/datasets/swg-camera-traps>, iUCN SSC Asian Wild Cattle Specialist Group's Saola Working Group.

Tabak, M.A. et al. (2019) Machine learning to classify animal species in camera trap images: Applications in ecology. *Methods Ecol. Evol.*, 10(4), 585–590.

van der Maaten, L. & Hinton, G. (2008) Visualizing data using t-SNE. *J. Mach. Learn. Res.*, 9, 2579–2605.

Vyskočil, J. & Picek, L. Towards zero-shot camera trap image categorization. In: *Proc. ECCV Workshops, 2024*, pp. 37–53, published 2025.

Weinstein, B.G. (2018) A computer vision for animal ecology. *Journal of Animal Ecology*, 87(3), 533–545.

WildHackers (2025) *Community fish detector*. GitHub, <https://github.com/WildHackers/community-fish-detector>.

Wildlife Conservation Society (2024) *WCS camera traps*. LILA BC, <https://lila.science/datasets/wcscameratraps>.

WWF (2024) *Living planet report 2024 – a system in peril*. World Wide Fund for Nature, Gland, Switzerland.

Yousif, H., Kays, R. & He, Z. (2019) Dynamic programming selection of object proposals for sequence-level animal species classification in the wild. <https://lila.science/datasets/ena24detection>.

Zhai, X. et al. Sigmoid loss for language image pre-training. In: *Proc. ICCV, 2023*, pp. 11301–11311.

Zhang, Z., He, Z., Cao, G. & Cao, W. (2016) Animal detection from highly cluttered natural scenes using spatiotemporal object region proposals and patch verification. *IEEE Trans. Multimedia*, 18(10), 2079–2092.

How to cite this article: Markoff H., Bengtson S.H., and Ørsted M.. Vision Transformers for Zero-Shot Clustering of Animal Images: A Comparative Benchmarking Study [Preprint]. February 2026. Not peer reviewed.

APPENDIX

A EVALUATION METRICS CALCULATIONS

This appendix provides the complete mathematical formulations and explanations for the clustering evaluation metrics used in this study.

V-measure balances homogeneity and completeness through their harmonic mean, preventing optimization shortcuts where

methods achieve high homogeneity by over-splitting or high completeness by collapsing all data into few clusters.

AMI quantifies information-theoretic agreement between predicted and ground truth partitions while correcting for chance agreement. Unlike raw mutual information or V-measure, AMI accounts for the fact that random clusterings achieve non-zero scores when compared to any partition. This adjustment is critical when comparing methods with vastly different cluster counts, as it prevents bias toward higher K values.

AMI serves as a secondary validation metric, particularly for unsupervised clustering methods where automatic cluster count determination may deviate substantially from $S = 30$.

A.1 Mathematical formulations

Let $\mathcal{C} = \{C_1, \dots, C_K\}$ denote predicted clusters and $\mathcal{G} = \{G_1, \dots, G_S\}$ denote ground truth species labels for N images. Define:

- $n_{ks} = |C_k \cap G_s|$: number of images in cluster k belonging to species s
- $n_k = |C_k| = \sum_s n_{ks}$: size of cluster k
- $n_s = |G_s| = \sum_k n_{ks}$: number of images of species s

A.1.1 Homogeneity

Homogeneity measures whether each cluster contains only members of a single species. It equals 1 when all clusters are “pure” (each contains exactly one species) and approaches 0 when clusters contain uniform mixtures of all species.

$$h = \begin{cases} 1 & \text{if } H(\mathcal{G}) = 0 \\ 1 - \frac{H(\mathcal{G}|\mathcal{C})}{H(\mathcal{G})} & \text{otherwise} \end{cases}$$

where entropy of ground truth labels is:

$$H(\mathcal{G}) = - \sum_{s=1}^S \frac{n_s}{N} \log \left(\frac{n_s}{N} \right)$$

and conditional entropy of ground truth given cluster assignments is:

$$H(\mathcal{G}|\mathcal{C}) = - \sum_{k=1}^K \sum_{s=1}^S \frac{n_{ks}}{N} \log \left(\frac{n_{ks}}{n_k} \right)$$

Ecological interpretation: High homogeneity means ecologists can confidently assign species labels to clusters with minimal validation. Low homogeneity indicates clusters contain multiple species, requiring more exhaustive manual review to avoid mislabeling.

A.1.2 Completeness

Completeness measures whether all members of a species are assigned to the same cluster. It equals 1 when each species occupies exactly one cluster and approaches 0 when every species is uniformly split across all clusters.

$$c = \begin{cases} 1 & \text{if } H(\mathcal{C}) = 0 \\ 1 - \frac{H(\mathcal{C}|\mathcal{G})}{H(\mathcal{C})} & \text{otherwise} \end{cases}$$

where entropy of cluster assignments is:

$$H(\mathcal{C}) = - \sum_{k=1}^K \frac{n_k}{N} \log \left(\frac{n_k}{N} \right)$$

and conditional entropy of clusters given ground truth is:

$$H(\mathcal{C}|\mathcal{G}) = - \sum_{s=1}^S \sum_{k=1}^K \frac{n_{ks}}{N} \log \left(\frac{n_{ks}}{n_s} \right)$$

Ecological interpretation: Low completeness means species images are scattered across multiple clusters, increasing validation burden. However, splits may reveal biologically meaningful subcategories (male/female dimorphism, juvenile/adult, seasonal pelage differences). Post-hoc inspection distinguishes informative fragmentation from pure failure.

A.1.3 V-Measure

V-measure is the harmonic mean of homogeneity and completeness, providing a balanced assessment:

$$V = 2 \cdot \frac{h \cdot c}{h + c}$$

The harmonic mean heavily penalizes imbalance. A method achieving $h = 0.95$, $c = 0.50$ yields only $V = 0.655$, not the arithmetic mean of 0.725. This prevents extreme over-splitting (high h , low c) or under-splitting (low h , high c).

Range: $V \in [0, 1]$, where $V = 1$ requires perfect clustering ($h = c = 1$).

A.1.4 Adjusted Mutual Information (AMI)

Mutual information quantifies shared information between clusterings:

$$MI(\mathcal{C}, \mathcal{G}) = \sum_{k=1}^K \sum_{s=1}^S \frac{n_{ks}}{N} \log \left(\frac{N \cdot n_{ks}}{n_k \cdot n_s} \right)$$

However, random clusterings achieve $MI > 0$ due to chance overlap. AMI corrects for this by subtracting expected MI under random permutation:

$$AMI(\mathcal{C}, \mathcal{G}) = \frac{MI(\mathcal{C}, \mathcal{G}) - \mathbb{E}[MI]}{\text{avg}(H(\mathcal{C}), H(\mathcal{G})) - \mathbb{E}[MI]}$$

Range: $AMI \in [0, 1]$ for similar cluster and species counts. Can be negative when clustering performs worse than random assignment.

Raw MI increases with cluster count, treating more clusters as more information, even if random. AMI corrects this bias.

When AMI and V-measure disagree: AMI is more sensitive to cluster count deviations. A method producing 90 clusters ($3 \times$ true count) may achieve high V-measure if splits occur within species (high homogeneity maintained), but lower AMI

due to information redundancy. In our experiments, AMI and V-measure correlated strongly ($r > 0.92$) for well-performing methods but diverged for pathological cases (DBSCAN with 200+ clusters), confirming their complementary roles.

B COMPLETE DATASET COMPOSITION

This appendix provides comprehensive details for all 60 species used in the study, including total image counts, validation status, and source datasets from LILA BC.

C SUPPLEMENTARY RESULTS

This appendix contains complete performance matrices for all experimental configurations tested in this study.

D EXTENDED CLUSTERING RESULTS FOR UNEVEN DISTRIBUTIONS

This appendix provides comprehensive clustering results for the extreme uneven distribution scenario discussed in Section 4.7. We systematically evaluated 10 parameter configurations for both HDBSCAN and DBSCAN, testing each with both t-SNE and UMAP dimensionality reduction.

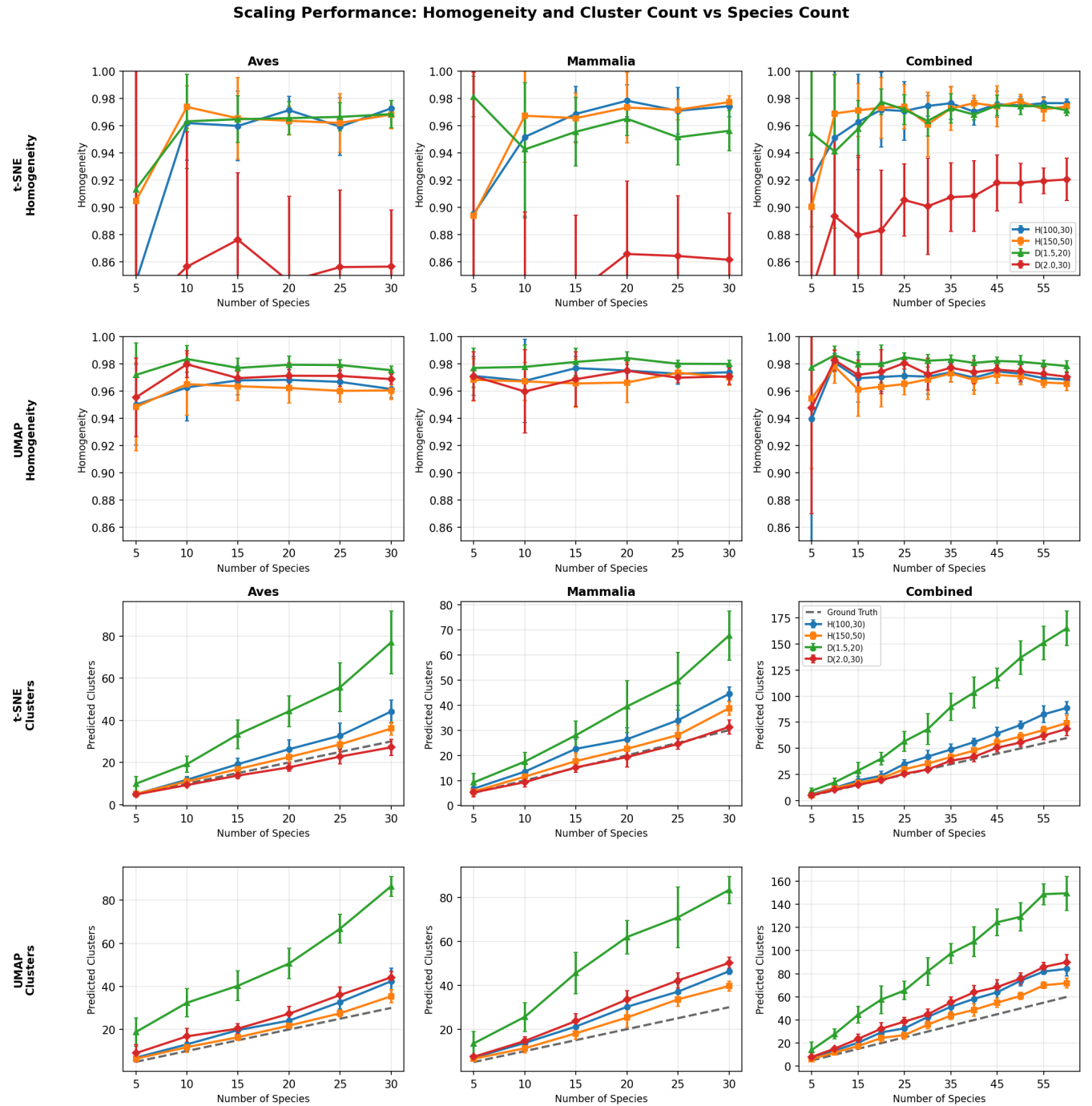


FIGURE D1 Scaling behavior of optimized clustering configurations across varying species counts (5–30 for single-class, 5–60 for combined). Left panels show V-measure, right panels show predicted cluster count. Top row: t-SNE dimensionality reduction. Bottom row: UMAP dimensionality reduction. Dashed diagonal lines indicate ideal cluster count prediction. H = HDBSCAN configurations, D = DBSCAN configurations. See Table D6 for detailed performance metrics at 30/60 species.

TABLE B1 Complete Species Dataset Composition (see Table 1 for source abbreviations)

#	Class	Species Name	Sources	Total	Valid	Uncertain
Aves (Birds) - 30 Species						
1	Aves	American crow (<i>Corvus brachyrhynchos</i>)	ICT,SIC,ENA	1,240	1,234	6
2	Aves	Australasian swamphen (<i>Porphyrio melanotus</i>)	NZC	2,772	2,772	0
3	Aves	Australian magpie (<i>Gymnorhina tibicen</i>)	ICT,NZC	2,739	2,733	6
4	Aves	Black curassow (<i>Crax alector</i>)	WCS	1,949	1,939	10
5	Aves	Blue whistling thrush (<i>Myophonus caeruleus</i>)	SWG,WCS	2,157	2,128	29
6	Aves	Brown quail (<i>Synoicus ypsilophorus</i>)	NZC	2,662	2,652	10
7	Aves	Chicken (<i>Gallus gallus domesticus</i>)	ISC,SIC,NZC,ENA	1,647	1,629	18
8	Aves	Common chaffinch (<i>Fringilla coelebs</i>)	NZC	2,384	2,370	14
9	Aves	Common myna (<i>Acridotheres tristis</i>)	NZC	2,707	2,704	3
10	Aves	Dunnock (<i>Prunella modularis</i>)	NZC	2,066	2,055	11
11	Aves	European starling (<i>Sturnus vulgaris</i>)	NZC	1,876	1,867	9
12	Aves	Fantails (<i>Rhipidura</i>)	NZC	2,127	2,121	6
13	Aves	Greenfinch (<i>Chloris chloris</i>)	NZC	2,503	2,483	20
14	Aves	Kea (<i>Nestor notabilis</i>)	NZC	2,833	2,814	19
15	Aves	Kiwi (<i>Apteryx</i>)	NZC	1,634	1,620	14
16	Aves	Kori bustard (<i>Ardeotis kori</i>)	SS24,SCD,SKA,SKG,SSE,WCS	1,485	1,484	1
17	Aves	Mountain quail (<i>Oreortyx pictus</i>)	NAC,NZC	2,381	2,337	44
18	Aves	New Zealand robin (<i>Petroica australis</i>)	SIC,NZC	2,753	2,719	34
19	Aves	Ostrich (<i>Struthionidae</i>)	SS24,SCD,SKA,SKG,SSE,SMZ	3,727	3,722	5
20	Aves	Petrel (<i>Procellariidae</i>)	ISC	2,370	2,354	16
21	Aves	Pipit (<i>Anthus</i>)	NZC	2,316	2,238	78
22	Aves	Red junglefowl (<i>Gallus gallus</i>)	SWG,WCS	2,684	2,671	13
23	Aves	Spix's guan (<i>Penelope jacquacu</i>)	WCS	3,032	3,022	10
24	Aves	Swamp harrier (<i>Circus approximans</i>)	NZC	2,917	2,917	0
25	Aves	Takahē (<i>Porphyrio mantelli</i>)	NZC	2,085	2,073	12
26	Aves	Tūī (<i>Prosthemadera novaeseelandiae</i>)	NZC	2,767	2,747	20
27	Aves	Vulturine guineafowl (<i>Acryllium vulturinum</i>)	WCS	4,420	4,412	8
28	Aves	Weka (<i>Gallirallus australis</i>)	NZC	2,421	2,411	10
29	Aves	Wild turkey (<i>Meleagris gallopavo</i>)	NAC,ENA	2,057	2,057	0
30	Aves	Yellow-eyed penguin (<i>Megadyptes antipodes</i>)	NZC	2,817	2,815	2
Aves Subtotal				72,528	72,070	458
Mammalia (Mammals) - 30 Species						
31	Mammals	Alpaca (<i>Vicugna pacos</i>)	WCS	1,864	1,864	0
32	Mammals	American black bear (<i>Ursus americanus</i>)	NAC,ENA,SIC,ICT	2,912	2,797	115
33	Mammals	Black rhinoceros (<i>Diceros bicornis</i>)	SMZ,DLC,WCS,SKA,SS24	1,428	1,419	9
34	Mammals	Black-backed jackal (<i>Lupulella mesomelas</i>)	DLC,SMZ,SKG,SSE,SS24,SCD,SKA,WCS	2,067	2,053	14
35	Mammals	Bushpig (<i>Potamochoerus larvatus</i>)	SCD,WCS,SMZ,SS24,NKC	1,241	1,230	11
36	Mammals	Common brushtail possum (<i>Trichosurus vulpecula</i>)	WLC,UNS,NZC	1,365	1,358	7
37	Mammals	Common raccoon (<i>Procyon lotor</i>)	SIC,WCS,NAC,OSU,CAL	2,700	2,577	123
38	Mammals	Crab-eating mongoose (<i>Urva urva</i>)	SWG,WCS	2,364	2,316	48
39	Mammals	Crested porcupine (<i>Hystrix cristata</i>)	WCS,SKR,SSE,SCD,ICT,SKA,SMZ,SKG,SS24	1,449	1,449	0
40	Mammals	Dromedary camel (<i>Camelus dromedarius</i>)	WCS	1,809	1,798	11
41	Mammals	Eastern gray squirrel (<i>Sciurus carolinensis</i>)	NAC,ENA	2,434	2,414	20
42	Mammals	Ferret badger (<i>Melogale</i>)	SWG	1,743	1,671	72
43	Mammals	Gemsbok (<i>Oryx gazella</i>)	SCD,SKA,SS24,SMZ,SKG,DLC	3,963	3,944	19
44	Mammals	Giant armadillo (<i>Priodontes maximus</i>)	WCS	463	461	2
45	Mammals	Giraffe (<i>Giraffa camelopardalis</i>)	SS24,SSE,DLC,SKR,WCS	2,985	2,974	11
46	Mammals	Greater kudu (<i>Tragelaphus strepsiceros</i>)	DLC,WCS,NKC	4,410	4,375	35
47	Mammals	Hippopotamus (<i>Hippopotamus amphibius</i>)	SKR,WCS,SSE,SS24	2,319	2,314	5
48	Mammals	Jaguar (<i>Panthera onca</i>)	WCS	6,855	6,831	24
49	Mammals	L'Hoest's monkey (<i>Allochrocebus lhoesti</i>)	WCS	2,941	2,921	20
50	Mammals	Least weasel (<i>Mustela nivalis</i>)	NZC	1,869	1,869	0
51	Mammals	New Zealand sea lion (<i>Phocartos hookeri</i>)	NZC	2,296	2,277	19
52	Mammals	Northern treeshrew (<i>Tupaia belangeri</i>)	SWG,WCS	699	687	12
53	Mammals	Serval (<i>Leptailurus serval</i>)	SSE,SS24,WCS,NKC,SKR	625	625	0
54	Mammals	Ship rat (<i>Rattus rattus</i>)	WLC	822	822	0
55	Mammals	Spotted pacific paca (<i>Cuniculus paca</i>)	WCS	1,715	1,673	42
56	Mammals	Stump-tailed macaque (<i>Macaca arctoides</i>)	SWG,WCS	3,558	3,535	23
57	Mammals	Sun bear (<i>Helarctos malayanus</i>)	WCS,SWG	713	709	4
58	Mammals	Warthog (<i>Phacochoerus africanus</i>)	SSE,SMZ,SS24,SKR	1,671	1,666	5
59	Mammals	White-nosed coati (<i>Nasua narica</i>)	WCS,SEN,MIS	1,996	1,988	8
60	Mammals	Wolf (<i>Canis lupus</i>)	ICT	2,307	2,307	0
Mammalia Subtotal				66,583	65,954	629
GRAND TOTAL (60 Species)				139,111	138,024	1,087

TABLE C2 Complete V-Measure Scores: All Model \times Dimension Reduction \times Clustering Combinations - Birds & Mammals

Model	Class	Dim. Reduction (Avg. All Clusterings)					Supervised K=30 (UMAP+t-SNE)		Unsupervised (UMAP+t-SNE)	
		UMAP	t-SNE	PCA	Isomap	KPCA	GMM	Hier.	HDBSCAN	DBSCAN
DINOv3	Birds	0.877	0.884	0.456	0.686	0.527	0.957	0.960	0.932	0.671
	Mammals	0.869	0.879	0.458	0.642	0.295	0.952	0.952	0.914	0.677
DINOv2	Birds	0.843	0.846	0.492	0.622	0.460	0.900	0.901	0.896	0.679
	Mammals	0.795	0.806	0.488	0.550	0.443	0.849	0.852	0.823	0.678
BioCLIP 2	Birds	0.732	0.737	0.269	0.396	0.279	0.765	0.767	0.745	0.662
	Mammals	0.669	0.684	0.212	0.357	0.246	0.698	0.701	0.680	0.627
CLIP	Birds	0.680	0.689	0.202	0.294	0.213	0.705	0.707	0.692	0.633
	Mammals	0.642	0.661	0.197	0.276	0.196	0.660	0.663	0.666	0.618
SigLIP	Birds	0.654	0.663	0.215	0.272	0.218	0.675	0.680	0.665	0.615
	Mammals	0.625	0.640	0.242	0.298	0.205	0.637	0.641	0.646	0.605

Abbreviations: KPCA = Kernel PCA; Hier. = Hierarchical Clustering; Bold = best per class per metric.

Dim. Reduction columns: Average V-Measure across all 4 clustering methods (GMM K=30, Hier. K=30, HDBSCAN, DBSCAN).

All values averaged across 100 runs (10 subsamples \times 10 dimensionality reduction parameter configurations).

TABLE C3 Supervised Clustering Performance: Effect of Cluster Count (K) on V-Measure and AMI

Model	Method	K=15		K=30		K=45		K=90		K=180		Best K
		V-M	AMI	V-M	AMI	V-M	AMI	V-M	AMI	V-M	AMI	
DINOv3	Hierarchical	0.801	0.788	0.909	0.908	0.880	0.878	0.810	0.807	0.753	0.749	30
	GMM	0.793	0.780	0.909	0.907	0.880	0.877	0.811	0.808	0.754	0.750	30
DINOv2	Hierarchical	0.740	0.726	0.838	0.833	0.825	0.820	0.769	0.762	0.721	0.713	30
	GMM	0.731	0.717	0.837	0.832	0.823	0.818	0.768	0.761	0.722	0.714	30
BioCLIP 2	Hierarchical	0.608	0.588	0.686	0.673	0.697	0.685	0.668	0.655	0.641	0.627	45
	GMM	0.599	0.579	0.685	0.672	0.693	0.681	0.665	0.652	0.640	0.626	45
CLIP	Hierarchical	0.563	0.540	0.634	0.617	0.652	0.637	0.639	0.623	0.619	0.603	45
	GMM	0.556	0.533	0.632	0.615	0.648	0.633	0.636	0.620	0.618	0.602	45
SigLIP	Hierarchical	0.542	0.519	0.614	0.596	0.633	0.617	0.623	0.606	0.606	0.589	45
	GMM	0.535	0.512	0.611	0.593	0.628	0.612	0.619	0.602	0.604	0.587	45

Ground Truth: 30 species. V-M = V-Measure, AMI = Adjusted Mutual Information. Averages across 10 runs with UMAP and t-SNE combined.

TABLE C4 Unsupervised Clustering: Cluster Count Prediction (Ground Truth: 30 Species) - Birds vs. Mammals

Model	Dim. Red.	Method	Birds (Aves)			Mammals (Mammalia)		
			Pred. Clust.	Range	V-Meas.	Pred. Clust.	Range	V-Meas.
DINOv3	t-SNE	HDBSCAN	33.2 \pm 2.5	(29–40)	0.948	37.4 \pm 3.0	(29–43)	0.939
DINOv3	t-SNE	DBSCAN	255.5 \pm 13.1	(224–278)	0.668	247.2 \pm 10.8	(211–270)	0.668
DINOv3	UMAP	HDBSCAN	47.3 \pm 5.0	(34–56)	0.917	57.1 \pm 4.4	(44–71)	0.890
DINOv3	UMAP	DBSCAN	204.0 \pm 12.3	(179–236)	0.674	189.4 \pm 9.3	(173–212)	0.687
DINOv2	t-SNE	HDBSCAN	33.8 \pm 2.4	(30–39)	0.903	44.9 \pm 4.3	(38–56)	0.843
DINOv2	t-SNE	DBSCAN	220.6 \pm 11.9	(199–247)	0.677	217.9 \pm 12.5	(198–246)	0.672
DINOv2	UMAP	HDBSCAN	38.9 \pm 2.6	(32–46)	0.889	54.5 \pm 4.4	(43–65)	0.802
DINOv2	UMAP	DBSCAN	172.7 \pm 10.8	(146–198)	0.680	149.0 \pm 11.2	(124–176)	0.685
BioCLIP 2	t-SNE	HDBSCAN	57.1 \pm 5.1	(46–69)	0.760	59.2 \pm 4.5	(45–66)	0.700
BioCLIP 2	t-SNE	DBSCAN	220.3 \pm 9.5	(201–239)	0.652	225.8 \pm 8.5	(204–246)	0.630
BioCLIP 2	UMAP	HDBSCAN	64.3 \pm 6.7	(43–80)	0.729	70.3 \pm 6.7	(55–86)	0.659
BioCLIP 2	UMAP	DBSCAN	136.8 \pm 8.7	(112–158)	0.672	150.4 \pm 7.8	(129–175)	0.625
CLIP	t-SNE	HDBSCAN	59.1 \pm 5.3	(48–69)	0.708	69.5 \pm 5.4	(58–79)	0.686
CLIP	t-SNE	DBSCAN	244.3 \pm 7.8	(228–265)	0.630	240.7 \pm 10.6	(219–265)	0.627
CLIP	UMAP	HDBSCAN	67.5 \pm 5.3	(51–80)	0.677	76.2 \pm 6.6	(54–90)	0.646
CLIP	UMAP	DBSCAN	140.9 \pm 9.3	(116–162)	0.637	162.0 \pm 9.6	(135–184)	0.610
SigLIP	t-SNE	HDBSCAN	61.8 \pm 5.1	(49–71)	0.681	70.2 \pm 6.8	(50–83)	0.661
SigLIP	t-SNE	DBSCAN	239.3 \pm 7.9	(226–254)	0.619	248.9 \pm 9.8	(228–267)	0.612
SigLIP	UMAP	HDBSCAN	68.2 \pm 7.0	(53–87)	0.648	77.3 \pm 6.9	(46–89)	0.631
SigLIP	UMAP	DBSCAN	154.5 \pm 9.5	(135–192)	0.611	166.9 \pm 10.1	(140–193)	0.598

Note: Predicted clusters shown as Mean \pm SD. Best cluster prediction (closest to 30) and V-Measure per class shown in bold.

All values averaged across 100 runs (10 subsamples \times 10 dimension reduction runs).

TABLE C5 Complete Clustering Metrics for Top-Performing Configurations at K=30: Birds vs. Mammals

Model	Dim. Red.	Clustering	Birds (Aves)						Mammals (Mammalia)					
			V-M	AMI	ARI	Hom.	Cmp.	Sil.	V-M	AMI	ARI	Hom.	Cmp.	Sil.
DINOv3	t-SNE	Hierarchical	0.961	0.960	0.943	0.961	0.961	0.714	0.954	0.953	0.919	0.953	0.956	0.685
DINOv3	t-SNE	GMM	0.958	0.957	0.927	0.956	0.960	0.708	0.954	0.953	0.914	0.951	0.956	0.679
DINOv3	UMAP	Hierarchical	0.960	0.959	0.941	0.959	0.960	0.868	0.949	0.948	0.907	0.947	0.951	0.821
DINOv3	UMAP	GMM	0.956	0.955	0.925	0.954	0.958	0.872	0.949	0.948	0.904	0.947	0.952	0.823
DINOv2	t-SNE	Hierarchical	0.903	0.900	0.834	0.900	0.905	0.711	0.855	0.852	0.742	0.851	0.860	0.630
DINOv2	t-SNE	GMM	0.900	0.898	0.827	0.897	0.903	0.700	0.853	0.850	0.723	0.848	0.859	0.618
DINOv2	UMAP	Hierarchical	0.900	0.898	0.829	0.898	0.903	0.857	0.848	0.845	0.719	0.843	0.854	0.744
DINOv2	UMAP	GMM	0.901	0.898	0.829	0.898	0.903	0.851	0.845	0.842	0.702	0.839	0.852	0.730
BioCLIP 2	t-SNE	Hierarchical	0.770	0.765	0.606	0.765	0.776	0.558	0.703	0.696	0.512	0.698	0.708	0.502
BioCLIP 2	t-SNE	GMM	0.767	0.762	0.588	0.761	0.774	0.554	0.703	0.696	0.506	0.696	0.709	0.496
BioCLIP 2	UMAP	Hierarchical	0.764	0.758	0.572	0.756	0.772	0.672	0.699	0.693	0.491	0.691	0.708	0.586
BioCLIP 2	UMAP	GMM	0.763	0.758	0.564	0.754	0.772	0.658	0.693	0.687	0.473	0.683	0.704	0.557
CLIP	t-SNE	Hierarchical	0.708	0.701	0.528	0.704	0.712	0.491	0.668	0.661	0.460	0.663	0.674	0.460
CLIP	t-SNE	GMM	0.709	0.702	0.523	0.704	0.714	0.487	0.665	0.657	0.450	0.658	0.671	0.451
CLIP	UMAP	Hierarchical	0.706	0.700	0.513	0.701	0.712	0.602	0.658	0.651	0.432	0.649	0.668	0.556
CLIP	UMAP	GMM	0.701	0.695	0.491	0.694	0.709	0.576	0.656	0.648	0.415	0.644	0.668	0.537
SigLIP	t-SNE	Hierarchical	0.678	0.671	0.479	0.673	0.683	0.466	0.644	0.636	0.439	0.639	0.648	0.455
SigLIP	t-SNE	GMM	0.675	0.667	0.469	0.669	0.680	0.468	0.642	0.635	0.435	0.637	0.648	0.455
SigLIP	UMAP	Hierarchical	0.682	0.674	0.474	0.675	0.689	0.568	0.638	0.629	0.418	0.630	0.645	0.534
SigLIP	UMAP	GMM	0.675	0.668	0.450	0.666	0.684	0.549	0.631	0.623	0.392	0.621	0.642	0.503

Metrics: V-M = V-Measure; AMI = Adjusted Mutual Info; ARI = Adjusted Rand Index; Hom. = Homogeneity; Cmp. = Completeness; Sil. = Silhouette Score.

All values averaged across 100 runs (10 subsamples \times 10 dimension reduction runs). Best value per metric per class shown in bold.

Note: Birds consistently achieve higher clustering performance than mammals across all models (avg. V-Measure difference: 0.042).

TABLE D6 Clustering performance on extreme uneven distributions (20-MAX images per species). Results averaged over 10 random samples. HDBSCAN(min_cluster_size, min_samples), DBSCAN($\epsilon \times$ multiplier, min_samples). Bold values indicate best V-measure per dimensionality reduction method.

Config	Aves (30 species)				Mammalia (30 species)				Combined (60 species)			
	V	H	Cl.	O%	V	H	Cl.	O%	V	H	Cl.	N%
<i>t-SNE</i>												
HDBSCAN(15,5)	0.776	0.977	415	14.2	0.792	0.978	304	12.2	0.798	0.985	781	15.9
HDBSCAN(30,10)	0.876	0.977	120	7.7	0.868	0.973	97	6.2	0.880	0.981	254	9.2
HDBSCAN(50,20)	0.921	0.972	58	4.7	0.907	0.975	57	3.9	0.922	0.976	124	5.0
HDBSCAN(75,25)	0.931	0.973	48	4.7	0.912	0.974	50	3.8	0.929	0.976	103	4.6
HDBSCAN(100,30)	0.936	0.974	43	4.7	0.918	0.973	44	3.9	0.936	0.977	91	4.2
HDBSCAN(150,50)	0.946	0.971	36	4.7	0.930	0.973	39	3.7	0.948	0.973	72	4.1
DBSCAN(1.0,10)	0.694	0.990	699	21.3	0.700	0.989	575	21.1	0.734	0.991	1197	21.6
DBSCAN(1.2,15)	0.813	0.983	226	8.2	0.817	0.982	176	8.2	0.830	0.985	436	9.1
DBSCAN(1.5,20)	0.909	0.972	75	2.3	0.887	0.963	68	2.1	0.900	0.972	167	2.8
DBSCAN(2.0,30)	0.911	0.872	28	0.3	0.899	0.877	32	0.2	0.930	0.922	68	0.5
<i>UMAP</i>												
HDBSCAN(15,5)	0.869	0.972	178	6.4	0.843	0.978	179	7.9	0.893	0.978	294	6.8
HDBSCAN(30,10)	0.897	0.968	91	4.6	0.878	0.977	95	5.5	0.912	0.976	164	5.1
HDBSCAN(50,20)	0.911	0.966	62	3.7	0.901	0.975	62	3.6	0.920	0.973	122	4.1
HDBSCAN(75,25)	0.916	0.964	51	3.3	0.910	0.975	52	3.1	0.926	0.971	102	3.4
HDBSCAN(100,30)	0.922	0.962	45	3.0	0.920	0.973	45	2.1	0.933	0.971	89	3.1
HDBSCAN(150,50)	0.933	0.955	36	2.3	0.926	0.971	40	1.9	0.942	0.967	74	2.3
DBSCAN(1.0,10)	0.763	0.984	382	19.3	0.753	0.987	347	21.9	0.814	0.986	608	21.9
DBSCAN(1.2,15)	0.855	0.979	161	7.2	0.826	0.984	159	10.1	0.871	0.984	284	10.7
DBSCAN(1.5,20)	0.910	0.974	80	2.9	0.877	0.979	85	3.9	0.910	0.980	155	4.3
DBSCAN(2.0,30)	0.940	0.964	45	1.6	0.914	0.967	50	1.1	0.939	0.973	95	1.6

Metrics: V = V-measure (harmonic mean of homogeneity and completeness), H = Homogeneity (each cluster contains only members of a single class), Cl. = Number of clusters found (true values: 30/30/60), O% = Percentage of points classified as outliers.